AD-A167 972 MOLECULAR DYNAMICS OF THE A + BC REACTION IN RARE GAS SOLUTION(U) CALIFORNIA UNIV SAN DIEGO LA JOLLA DEPT OF CHEMISTRY J P BERGSMA ET AL. 01 MAY 86 1/1

UNCLASSIFIED N00014-78-C-0325 F/G 7/4 NL

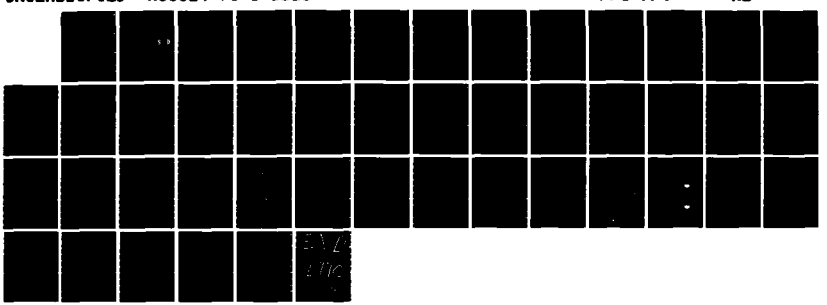

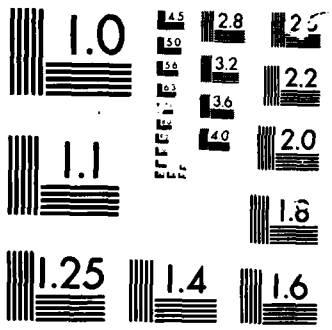
1.0
1.1
1.25
1.4
1.6
1.8
2.0
2.2
2.8
3.2
3.6
4.0
4.5
5.0
5.6
6.3
MICROCOPY
CHART

(12)

OFFICE OF NAVAL RESEARCH

Contract N00014-78-C-0325

TECHNICAL REPORT

MOLECULAR DYNAMICS OF THE A + BC REACTION IN RARE GAS SOLUTION

by

John P. Bergsma, Jeffrey R. Reimers, Kent R. Wilson*
James T. Hynes +

Prepared for Publication

in

Journal of Chemical Physics

*Department of Chemistry, University of California, San Diego, La Jolla, CA 92093
+Department of Chemistry, University of Colorado, Boulder, CO 80309

May 1, 1986

SECURITY CLASSIFICATION OF THIS PAGE (When Data Entered)

REPORT DOCUMENTATION PAGE		READ INSTRUCTIONS BEFORE COMPLETING FORM
1. REPORT NUMBER N00014-78-C-0325	2. GOVT ACCESSION NO.	3. RECIPIENT'S CATALOG NUMBER
4. TITLE (and Subtitle) Molecular Dynamics of the A + BC Reaction in Rare Gas Solution		5. TYPE OF REPORT & PERIOD COVERED Technical Report 6. PERFORMING ORG. REPORT NUMBER
7. AUTHOR(s) John P. Bergsma, Jeffrey R. Reimers, Kent R. Wilson, James T. Hynes		8. CONTRACT OR GRANT NUMBER(s) N00014-78-C-0325
9. PERFORMING ORGANIZATION NAME AND ADDRESS THE REGENTS OF THE UNIVERSITY OF CALIFORNIA University of California, San Diego La Jolla, California 92093		10. PROGRAM ELEMENT, PROJECT, TASK AREA & WORK UNIT NUMBERS
11. CONTROLLING OFFICE NAME AND ADDRESS Office of Naval Research 800 North Quincy Street Arlington, Virginia 22217		12. REPORT DATE May 1, 1986 13. NUMBER OF PAGES 42
14. MONITORING AGENCY NAME & ADDRESS(if different from Controlling Office) Office of Naval Research Resident Representative Mail Code A-043 University of California, San Diego La Jolla, California 92093		15. SECURITY CLASS. (of this report) Unclassified 15a. DECLASSIFICATION/DOWNGRADING SCHEDULE

16. DISTRIBUTION STATEMENT (of this Report)

Approved for public release; distribution unlimited.

17. DISTRIBUTION STATEMENT (of the abstract entered in Block 20, if different from Report)

18. SUPPLEMENTARY NOTES

The views, opinions, and/or findings contained in this report are those of the author(s), and should not be construed as an official Department of the Navy position, policy, or decision, unless so designated by other documentation.

19. KEY WORDS (Continue on reverse side if necessary and identify by block number)

20. ABSTRACT (Continue on reverse side if necessary and identify by block number)

Molecular dynamics are computed for model atom transfers A+BC+C in rare gas solvents at liquid densities. We find that the reaction dynamics can be understood in terms of a simple picture which consists of three stages: 1) activation of reactants, 2) barrier crossing, and 3) deactivation of products. The effects seen in stages 1) and 3) can be largely interpreted in terms of existing models of energy and phase decay in solution, while the effects seen in stage 2) can be largely interpreted in terms of gas phase A+BC barrier crossing dynamics.

(OVER)

DD FORM 1 JAN 73 1473 EDITION OF 1 NOV 65 IS OBSOLETE

SECURITY CLASSIFICATION OF THIS PAGE (When Data Entered)

MOLECULAR DYNAMICS OF THE A + BC REACTION IN RARE GAS SOLUTION

John P. Bergsma, Jeffrey R. Reimers[a], *Kent R. Wilson*

Department of Chemistry
University of California, San Diego
La Jolla, CA 92093

James T. Hynes

Department of Chemistry
University of Colorado
Boulder, CO 80309

ABSTRACT

Molecular dynamics are computed for model atom transfers A + BC → AB + C in rare gas solvents at liquid densities. We find that the reaction dynamics can be understood in terms of a simple picture which consists of three stages: 1) activation of reactants, 2) barrier crossing, and 3) deactivation of products. The effects seen in stages 1) and 3) can be largely interpreted in terms of existing models of energy and phase decay in solution, while the effects seen in stage 2) can be largely interpreted in terms of gas phase A + BC barrier crossing dynamics. We find that Transition State Theory is in perfect agreement with the simulations for the 20 and 10 kcal/mol barrier reactions and is a very good description for a 5 kcal/mol reaction barrier. At low barrier curvature dynamical effects due to the solvent are shown to induce some recrossings of the transition state barrier, thus causing rate constants calculated by simple transition state theory to be slightly too high. A modification of transition state theory, which considers the effect of the time dependent friction of the solvent on the dynamics at the transition state, is shown to predict corrections to the rate constants in very good agreement with the results from the simulations.

Submitted to J. Chem. Phys.

a) Present address: Department of Theoretical Chemistry, F11, University of Sydney, N.S.W., 2006, Australia.

MOLECULAR DYNAMICS OF THE A + BC REACTION IN RARE GAS SOLUTION

John P. Bergsma, Jeffrey R. Reimers[a)], *Kent R. Wilson*

Department of Chemistry
University of California, San Diego
La Jolla, CA 92093

James T. Hynes

Department of Chemistry
University of Colorado
Boulder, CO 80309

I. Introduction

The simplest chemical reaction involving the making and breaking of different chemical bonds is the triatomic atom transfer reaction A + BC → AB + C. Its experimental and theoretical study[1] has been central to the detailed understanding of gas phase[2-7] reactions, contributing for example to the development of Transition State Theory (TST)[1,8] – which gives in many cases a clear and accurate picture of gas phase reaction kinetics – and to the development of Molecular Dynamics (MD) to understand the detailed microscopic motions involved in reactions. While the theoretical understanding of the microscopic processes of gas phase reactions is now well advanced, the corresponding understanding of the detailed aspects of reactions in liquid solution is still sketchy, in spite of what is arguably the greater relative importance of solution reactions in chemistry. (For reviews, see Refs. 8,10-15.)

The present work is, to our knowledge, the first full scale molecular dynamics study[9] of the A + BC reaction in solution in which reactive trajectories are computed. We analyze the resulting classical trajectories to try to answer some important questions about the nature of the A + BC reaction in solution, including:

1) What is the character of ABC trajectories that lead to reaction, and what is the solvent influence thereon? We find that these trajectories, except at the barrier top, are quite different in the solution and gas phases and, away from the barrier, can be characterized in terms of energy transfer and phase decay characteristics of various (eg. translational, rotational, vibrational) degrees of freedom of the nascent reactant and product species. In addition, the role of the solvent momenta in the reaction process is examined through solvent momentum perturbation calculations.

2) When is TST valid[8-15] in solution? The most apparently vulnerable feature of simple TST is the assumption that trajectories originating from reactants and achieving activation energy will always go on directly to form products with no recrossings of the transition state.[4] Clearly, this assumption is in jeopardy if the situation arises in which a strongly-interacting solvent impedes successful barrier crossing through "collisions" with the reacting complex near the transition state, thereby inducing recrossings and reducing the rate constant below the TST value. One might term this a dynamic solvent "cage" effect in the transition state neighborhood. We examine this question in some detail, and analyze our results in terms of the Grote-Hynes perspective of a time dependent friction[16-18] that the solvent exerts on the reaction coordinate in the neighborhood of the transition state, and its effect on the rate constant.

The appealing feature of TST is the simple but intuitive picture it gives for understanding the nature of reactive barrier passage: an activated complex, in quasi-equilibrium with reactants, proceeds directly to form products. A critical assumption of TST – the existence of an equilibrium between reactants and activated complexes – can be realized in a solvent where continual collisions occur with the reacting system, although these same interactions might sometimes cause the no-recrossing

condition to break down. If a trajectory recrosses the transition state surface then TST will overestimate the rate constant because it assumes that every crossing of the barrier toward products contributes to the overall rate. This recrossing effect is accounted for by the so called transmission coefficient κ correction to Transition State Theory. As is well known, the actual rate constant k is thus written in terms of the simple TST rate constant k^{TST} as

$$k = k^{TST}\,\kappa\,, \tag{1.1}$$

where κ adjusts the TST result to correct for the solvent induced recrossings. Some basic ingredients which determine κ are considered in a highly idealized treatment of reactions in solution by Kramers,[19] in which the reacting system is modeled as an effective particle of mass μ moving, in the transition state region, on an inverted parabolic potential of imaginary frequency whose real magnitude is ω_b, and subject to solvent friction ζ. The latter is defined in terms of the time correlation function of the random force exerted by the solvent on the reaction coordinate,

$$\zeta = \int_0^\infty dt\;\zeta(t)\,, \tag{1.2}$$

in which $\zeta(t)$ is given by the fluctuation-dissipation theorem as

$$\zeta(t) = \frac{1}{\mu k_B T}\langle\, FF(t)\,\rangle\,, \tag{1.3}$$

where F is the solvent force on the effective particle of mass μ and $\langle\ \rangle$ indicates a solvent phase-space average, k_B is Boltzmann's constant and T is the temperature. The Kramers theory emphasizes the key parameter ζ / ω_b in the determination of κ. If the frictional forces are weak compared to the intrinsic reaction forces acting on the particle in the barrier region, then $\zeta / \omega_b << 1$, $\kappa \to 1$ and $k \to k^{TST}$. If, on the other hand, the barrier curvature is very small and the retarding influence of the solvent is large, then $\zeta / \omega_b >> 1$ and $\kappa \to \omega_b / \zeta$. In this limit the solvent is very effective in inducing recrossings and the passage from reactants to products over the barrier is essentially diffusion-controlled.

In the latter case, and in regimes approaching it, the reaction rate is affected by the long time macroscopic friction in the Kramers description. There are, however, important cases for which this simple picture due to Kramers breaks down. It has been argued by Grote and Hynes[16-18] that TST can in fact be a good approximation, even for strong friction, if the barrier curvature is very sharp. For this case the reacting system spends so little time on the barrier (on the order of time ω_b^{-1}) that the solvent is unable to respond to, and retard motion across the barrier since there is not enough time for any effective collisions to occur. The effective solvent friction at the transition state is small because the short time scale solvent response, given by the early part of the time dependent friction, $\zeta(t)$, is more important[18] than the long-time overall response, ζ. We will see that this is an especially important perspective for sharp barriers.

The solvent can also play another important and quite distinct role; dissipating the excess energy of newly formed products. If energy deactivation of products is achieved a short time after the transition state is crossed, then it is unlikely that there will remain sufficient energy to recross the barrier: this helps TST to correctly describe the reaction. Conversely, the lack of sufficiently rapid energy transfer will lead to barrier recrossing by the energetically "hot" nascent products. In this event, the rate constant would depend on the rate of energy stabilization of the nascent products by the solvent.

Similar to the role that the solvent plays in the energy deactivation of products is the role it plays in providing energy for the activation of reactants. It is conceivable, for example, that this activation might be slow compared to the barrier passage step, so that activation dynamics explicitly enter the rate. It is also possible that only a small amount of solvent phase space can be effective in the activation of the reactants to form products.

One purpose of this paper is to investigate the validity of Transition State Theory for atom transfer reactions in monatomic liquids. We simulate reactions using molecular dynamics and explore a range of the system's properties (characterized by $\zeta(t)$, ω_b, etc...), discovering both where TST can be applied successfully and where it breaks down. In addition, we search for a simple picture to understand the reaction molecular dynamics, and begin the process of investigating the detailed role of the solvent

in affecting the course of the reaction.

The outline of the paper is as follows. In Sec. II we present in detail the computational techniques used to simulate A + BC trajectories in rare gas solvents. Section III explores the reaction $X + X_2$ in argon solvent. In Sec. IV we examine the effect of varying the nature of the solvent. Concluding remarks are given in Sec. V.

II. Computational Techniques

Molecular dynamics techniques have been previously used in several condensed phase reaction simulations; examples include defect motion in solids,[20,21] isomerization[22] and radical recombination[23,24] in solution, transformations in macromolecules,[25,26] and adsorption on surfaces.[27] The solution phase MD simulation of the A + BC reaction requires special attention to initial sampling and trajectory techniques which we now discuss.

A. Molecular Dynamics

Molecular dynamics are used to compute time histories of the positions and momenta for all of the atoms in the system. This is accomplished by numerical integration of the equations governing the classical motions of particles in a conservative force field, *i.e.* Hamilton's equations:

$$\dot{\mathbf{r}}^N = \frac{\partial H}{\partial \mathbf{p}^N} , \tag{2.1}$$

and

$$\dot{\mathbf{p}}^N = -\frac{\partial H}{\partial \mathbf{r}^N} , \tag{2.2}$$

in which $\mathbf{p}^N$ and $\mathbf{r}^N$ are the conjugate momentum and position for a system containing N unique particles, and H is the Hamiltonian for the system. Given a set of position coordinates, $\mathbf{r}^N$, the force on any particular atom is computed as the sum of the forces over all pairwise additive interactions, and a 3-body term is used to describe the internal A + BC interaction (see below). A modified Verlet algorithm,[28-30] incorporating a time step of 1.0 femtosecond, is used to integrate these equations of motion, and truncated octahedron periodic boundary conditions[31] are used in order to approximate an infinite liquid. There are 100 rare gas solvent atoms used in the liquid simulations.

These calculations are carried out on a Floating Point Systems AP120B array processor[32] attached to a VAX 11/780 host computer. One thousand time steps require approximately 100 seconds of real time on the array processor. The calculations presented here required 15 days of array processor time, and would have required 17 months of VAX 11/780 time if the array processor were not used.

B. Potential Energy Surface

In explicitly constructing the Hamiltonian in Eqs. (2.1) and (2.2), a potential energy surface is needed to describe the interactions between all of the atoms in the system. The potential energy surface used here is intended to represent a liquid-phase rare-gas solvent in which the symmetric A + BC hypothetical atom transfer reaction, $X + X_2 \rightarrow X_2 + X$, occurs. The X atoms are modeled as uncharged halogen-like atoms with the mass of chlorine 35. We stress that this is a *hypothetical model* of a symmetric atom transfer (The actual interhalogen transfer reactions appear to often involve low barriers and bound intermediates.[3]).

We choose a surface constructed as a combination of hypo-surfaces representing smaller parts of the problem. First, the potential energy of the interaction between any atom, i, and any solvent atom, j, is represented by the Lennard-Jones 6-12 potential

$$\Phi^{LJ}(r_{ij}) = 4\varepsilon_{ij}\left[\left[\frac{\sigma_{ij}}{r_{ij}}\right]^{12} - \left[\frac{\sigma_{ij}}{r_{ij}}\right]^{6}\right], \tag{2.3}$$

in which r_{ij} is the distance between the atoms, ε_{ij} is the depth of the minimum in the potential and σ_{ij} locates the finite intermolecular distance at which $\Phi^{LJ}(r_{ij}) = 0$. The values of ε_{ij} and σ_{ij} used for

various rare gas[33] and X-X interactions[34,35] in these calculations are given in Table 1. Table 1 gives parameters only for the homonuclear pair interactions. For the heteronuclear interactions the values of ε_{ij} and σ_{ij} are calculated using the combining rules

$$\varepsilon_{ij} = (\varepsilon_{ii}\,\varepsilon_{jj})^{1/2}\,, \tag{2.4}$$

$$\sigma_{ij} = (\sigma_{ii} + \sigma_{jj})\,/\,2\,. \tag{2.5}$$

Table 1. Lennard-Jones Parameters

$$4\varepsilon_{ij}\left[\left(\frac{\sigma_{ij}}{r_{ij}}\right)^{12} - \left(\frac{\sigma_{ij}}{r_{ij}}\right)^{6}\right]$$

Atom - Atom Interaction	σ_{ij} (Å)	ε_{ij} (J/mol)	ε/k_B (°K)
He - He	2.57	89.79	10.80
Ar - Ar	3.40	997.48	120.00
Xe - Xe	3.85	2077.20	249.83
X - X (X = Cl)	3.12	2868.68	345.02

Second, the potential energy function used for the X-X-X interaction is the 3-body London-Eyring-Polanyi-Sato (LEPS)[5] surface

$$\Phi^{LEPS}(r_1,r_2,r_3) = Q_1 + Q_2 + Q_3 - (J_1^2 + J_2^2 + J_3^2 - J_1J_2 - J_2J_3 - J_3J_1)^{1/2}\,, \tag{2.6}$$

in which r_1 and r_2 are the variable bond lengths between the "middle" X atom and the two "outside" X atoms, r_3 is the bond length between the two "outside" X atoms, and Q_i and J_i are linear combinations of the "singlet" and "triplet" diatomic energies:

$$Q_i(r_i) = ({}^1E_i + {}^3E_i)/2\,, \tag{2.7}$$

and

$$J_i(r_i) = ({}^1E_i - {}^3E_i)/2\,. \tag{2.8}$$

Here the "singlet" ground state energy is represented as a Morse potential,

$${}^1E_i(r_i) = {}^1D_i\left\{1 - \exp\left[-{}^1\beta_i(r_i - {}^1r_i^0)\right]\right\}^2 - {}^1D_i\,, \tag{2.9}$$

while the "triplet" diatomic energy is an anti-Morse potential,

$${}^3E_i(r_i) = {}^3D_i\left\{1 + \exp\left[-{}^3\beta_i(r_i - {}^3r_i^0)\right]\right\}^2 - {}^3D_i\,. \tag{2.10}$$

The LEPS potential is an analytic form, convenient for use in molecular dynamics simulations, which displays excellent asymptotic properties, reducing to a diatomic bound Morse potential when one atom is infinitely separated. In addition, it is highly adaptable, containing 18 non-symmetry adapted parameters (${}^1D_i$, ${}^3D_i$, ${}^1\beta_i$, ${}^3\beta_i$, ${}^1r_i^0$, ${}^3r_i^0$, for i = 1,2,3), allowing the simultaneous adjustment of barrier height and barrier frequency ω_b (*i.e.* the magnitude of the imaginary frequency of an inverted parabolic approximation to the potential at the saddle point for a linear geometry). We report all frequencies, ω_b, in spectroscopic units, *i.e.* $(\omega_b / 2\pi c)$ cm^{-1}. Table 2 shows the values of the 18 LEPS parameters used in these simulations, producing potentials with specific barrier heights and frequencies. In all cases, the X_2 diatomic potential in the limit of the X atom far away is a Morse potential fitted to the Cl_2 diatomic potential.[36] Figure 1 illustrates potential energy contours for a 20 kcal/mol barrier height and linear geometry. The coordinate axes are inclined at an angle of 60° rather than 90° since, for the X_3 system, this choice of axes diagonalizes the kinetic energy.[1] The equations of motion of the reaction system are

Table 2. X_3 LEPS Potential Parameters			
Barrier Height (kcal/mol)	20	10	5
Barrier Frequency (cm^{-1})	419	288	168
${}^1r_i^0$ (Å) i = 1,2,3	1.9870	1.9870	1.9870
${}^3r_i^0$ (Å) i = 1,2,3	1.9870	1.9870	1.9870
${}^1\beta_i$ ($Å^{-1}$) i = 1,2,3	2.0024	2.0024	2.0024
${}^3\beta_i$ ($Å^{-1}$) i = 1,2,3	2.0024	2.0024	2.0024
${}^1D_i$ (kcal/mol) i = 1,2,3	57.9740	57.9740	57.9740
${}^3D_i$ (kcal/mol) i = 1,2,3	44.2290	32.3965	27.2053

thus represented by a particle with point mass μ sliding on the potential energy surface.

C. Initial Conditions

The reaction coordinate of $X + X_2 \rightarrow X_2 + X$ in the barrier neighborhood is well defined by the asymmetric-stretch normal mode coordinate of X-X-X, while the magnitude of the corresponding imaginary normal mode frequency is the barrier frequency, ω_b. Other vibrational degrees of freedom for X_3 are described by the bend and symmetric-stretch normal modes.

If we attempted to discover a set of reactive trajectories by starting with reactants and solvent in equilibrium, we would have exhausted the capacity of the fastest available computer long before arriving at our answer. Therefore we use the technique of Keck[37,38] and Anderson[39,40] to initialize the trajectory from an equilibrium distribution of all variables except the position along the reaction coordinate which is constrained to the transition state surface. We compute the dynamics both forward and backward in time,[9,41] thus determining if the trajectory is reactive or unreactive. The precise nature of this equilibrium distribution on the barrier is highly dependent on the details of the potential energy surface at the barrier top. Here, the initial conditions for X_3 are determined by Boltzmann-weighted sampling of positions and momenta in the appropriate degrees of freedom described by the normal modes. The initial conditions are chosen to optimize the calculation of the ensemble-averaged values of the properties of interest. An ensemble average, $\langle A \rangle$, is defined classically as

$$\langle A \rangle = \frac{\iint d\mathbf{r}^N d\mathbf{p}^N \, A \, e^{-H(\mathbf{r}^N,\mathbf{p}^N)/k_BT}}{\iint d\mathbf{r}^N d\mathbf{p}^N \, e^{-H(\mathbf{r}^N,\mathbf{p}^N)/k_BT}} , \tag{2.11}$$

where $\mathbf{r}^N$ is a vector of the N Cartesian coordinates of the system, $\mathbf{p}^N$ is a vector of the momentum coordinates conjugate to $\mathbf{r}^N$, $H(\mathbf{r}^N,\mathbf{p}^N)$ is the full system Hamiltonian, k_B is Boltzmann's constant and T is the temperature. We select $\mathbf{r}^N$ and $\mathbf{p}^N$ from a Boltzmann distribution on the transition state surface. For the case of a solvent interacting weakly with the X_3, the transition state can be conveniently defined as lying along the symmetric stretch and bend coordinates passing through the lowest lying saddle point on the gas phase LEPS potential surface of X_3. We now turn to the details of the initial condition sampling.

1. Hamiltonian Separation

The reaction system coordinates comprise a set of "fast" degrees of freedom, q, associated with the X_3 vibrational normal mode coordinates and the remaining "slow" degrees of freedom, R, characteristic of the solvent translational motion and the rotational and translational motions of X_3. In the spirit of the familiar Born-Oppenheimer approximation for separation of nuclear and electronic motions, the Hamiltonian appropriate for our initial sampling is written as

$$H(\mathbf{r}^N,\mathbf{p}^N) = H(\mathbf{q},\mathbf{p},\mathbf{R},\mathbf{P}) \approx H_1(\mathbf{q},\mathbf{p};\mathbf{R}) + H_2(\mathbf{R},\mathbf{P};\bar{\mathbf{q}}) , \tag{2.12}$$

in which p and P are momenta pertinent to q and R respectively, $H_1(\mathbf{q},\mathbf{p};\mathbf{R})$ is the Hamiltonian for X_3 which is parametrically dependent on the solvent coordinates R, and $H_2(\mathbf{R},\mathbf{P};\bar{\mathbf{q}})$ is the Hamiltonian for the solvent which is parametrically dependent on the average value of the X_3 vibrational coordinates, $\bar{\mathbf{q}}$. If necessary, this formalism may be generalized[42] to allow for quantization of the fast variables q.

In the limit of weak coupling between X_3 and the solvent, we can ignore the parametric dependence of H_1 on the liquid coordinates R, and H_1 reduces to the X_3 gas phase Hamiltonian $H_1(\mathbf{q},\mathbf{p})$. The solvent Hamiltonian, H_2, is parametrically dependent on $\bar{\mathbf{q}}$ which we take as $\mathbf{q}_{eq}$, the coordinates of the saddle point. Thus, in the weak-coupling limit, H becomes

$$H(\mathbf{q},\mathbf{p},\mathbf{R},\mathbf{P}) \approx H_1(\mathbf{q},\mathbf{p}) + H_2(\mathbf{R},\mathbf{P};\mathbf{q}_{eq}) . \tag{2.13}$$

The problems associated with a molecular dynamics evaluation of any ensemble average, such as Eq. (2.11), are that standard random sampling techniques give a poor sampling of the sensitive variables q, and many different initial conditions must be sampled for proper convergence. In addition, random sampling techniques do little to provide physical insight into the regions of phase space which contribute most to the integral and, therefore, are important into the overall "chemistry" of the process. For example, the lowest lying saddle point on the LEPS potential surface occurs for linear X-X-X. This may, at first, lead one to believe that the most probable configuration for a reactive trajectory would be a collinear arrangement of X-X-X, as this requires a minimum of activation energy to cross the barrier. However a significantly bent configuration is actually the most probable arrangement of X-X-X; this is due to the entropic effect of more volume in configuration space at bent geometries and compensates for the increased activation energy required. In fact, the probability for an exactly linear configuration is zero. We will take this feature into account in what follows.

The distinction between the fast and slow variables in the system, as well as the assumption that there is weak coupling between the X_3 moiety and the solvent, allows us to choose initial conditions for the X_3 fast (*i.e.* vibrational) coordinates, q, independently of the choice of initial conditions for the remaining slow variables, R, (*i.e.* solvent translation, X_3 translation and rotation). In addition, classically, the initial conditions for momentum variables can be selected independently of the position coordinates. We choose an integration scheme which takes advantage of the parametric dependencies in Eq. (2.13) allowing us to determine initial conditions separately for the X_3 and for the solvent, taking the parametric degrees of freedom into account in an average way. A good approximation to Eq. (2.11) useful for generating a quadrature scheme thus is

$$\langle A \rangle \approx \frac{\int d\mathbf{q}d\mathbf{p}\, J(\mathbf{q},\mathbf{p})\, e^{-H_1(\mathbf{q},\mathbf{p})/k_BT} \int d\mathbf{R}d\mathbf{P}\, e^{-H_2(\mathbf{R},\mathbf{P};\mathbf{q}_{eq})/k_BT}\, A(\mathbf{q},\mathbf{p},\mathbf{R},\mathbf{P})}{\int d\mathbf{q}d\mathbf{p}\, J(\mathbf{q},\mathbf{p})\, e^{-H_1(\mathbf{q},\mathbf{p})/k_BT} \int d\mathbf{R}d\mathbf{P}\, e^{-H_2(\mathbf{R},\mathbf{P};\mathbf{q}_{eq})/k_BT}} . \tag{2.14}$$

We write the X_3 Hamiltonian as

$$H_1(\mathbf{q},\mathbf{p}) = \Phi_1(\mathbf{q}) + T_1(\mathbf{p}) \tag{2.15}$$

and the solvent Hamiltonian as

$$H_2(\mathbf{R},\mathbf{P};\mathbf{q}_{eq}) = \Phi_2(\mathbf{R};\mathbf{q}_{eq}) + T_2(\mathbf{P}) , \tag{2.16}$$

in which $\Phi_1(\mathbf{q})$ is the gas phase potential energy (LEPS) of the X_3 reaction system, $\Phi_2(\mathbf{R};\mathbf{q}_{eq})$ is the solvent potential energy which is parametrically dependent on $\mathbf{q}_{eq}$, $T_1(\mathbf{p})$ is the vibrational kinetic energy of X_3, $T_2(\mathbf{P})$ is the solvent translational kinetic energy plus X_3 translational and rotational kinetic energy, and $J(\mathbf{q},\mathbf{p})$ is the Jacobian which is yet to be determined for transformation from Cartesian

variables to the internal vibrational coordinates, q, of X_3. Eq. (2.14) is evaluated using a product quadrature in which the q, p, R, and P coordinates are chosen independently: P by a Gaussian random number generator, R by molecular dynamics, and q and p by product Gauss-Hermite quadrature in the internal coordinates (see below). Note, however, that the quadrature scheme used provides a formally exact evaluation of Eq. (2.11) in the limit of an infinite number of trajectories. The approximation used in generating the quadrature only slows the convergence.

2. Effective LEPS Potential

The integral in the ensemble average Eq. (2.14) over the X_3 vibrational degrees of freedom can now be written as

$$\int dq dp\, J(q,p)\, e^{-H_1(q,p)/k_BT} = \left[\int dq\, J(q)\, e^{-\Phi_1(q)/k_BT}\right]\left[\int dp\, e^{-T_1(p)/k_BT}\right], \tag{2.17}$$

where we choose q to be the normal coordinates of X_3 and choose p independently of q so that $J(q,p)$ is only a function of q. The gas phase LEPS potential for X_3 can be conveniently written as a function of the X_3 valence coordinates r_1, r_2, and θ, in which r_1 and r_2 are the bond lengths between the center atom and the outer two atoms respectively, and $0 \le \theta \le \pi$ is the X-X-X bend angle. Introducing these variables allows us to evaluate the Jacobian, and thus write the integration over internal position coordinates in Eq. (2.17) as

$$\begin{aligned}\int dq\, J(q)\, e^{-\Phi_1(q)/k_BT} &= 8\pi^2 V \int_0^\infty dr_1 \int_0^\infty dr_2 \int_0^\pi d\theta\, J(r_1,r_2,\theta)\, e^{-\Phi^{LEPS}(r_1,r_2,\theta)/k_BT} \\ &= 8\pi^2 V \int_0^\infty dr_1 \int_0^\infty dr_2 \int_0^\pi d\theta\, r_1^2 r_2^2 \sin\theta\, e^{-\Phi^{LEPS}(r_1,r_2,\theta)/k_BT},\end{aligned} \tag{2.18}$$

where V is the volume. If we write an "entropy-corrected" potential as

$$\Phi'(r_1,r_2,\theta) = \Phi^{LEPS}(r_1,r_2,\theta) - k_BT\, ln[J(r_1,r_2,\theta)/J(r_1^e,r_2^e,\theta^e)], \tag{2.19}$$

in which $J(r_1^e,r_2^e,\theta^e)$ removes the dimensionality in ln, then Eq. (2.18) becomes

$$\int dq\, J(q)\, e^{-\Phi_1(q)/k_BT} = J(r_1^e,r_2^e,\theta^e)\, 8\pi^2 V \int_0^\infty dr_1 \int_0^\infty dr_2 \int_0^\pi d\theta\, e^{-\Phi'(r_1,r_2,\theta)/k_BT}. \tag{2.20}$$

Figure 2 shows the shape of the potentials $\Phi'(r_1,r_2,\theta)$, $\Phi^{LEPS}(r_1,r_2,\theta)$ and the function $-k_BT\, ln[J(r_1,r_2,\theta)/J(r_1^e,r_2^e,\theta^e)]$ versus angle θ for $r_1 = r_2 = 2.254$ Å, $r_1^e = r_1$, $r_2^e = r_2$, $\theta^e = 90°$ (*i.e.*, $\sin(\theta^e) = 1$), and LEPS potential parameters defining the 20 kcal/mol barrier (see Table 2). For these parameters the minimum in energy of $\Phi'(\theta)$ occurs at $\theta = 148.5°$. The use of internal coordinate variables and the effective potential, Φ', has given us some insight into the nature of the most important position coordinates at the saddle point; we now see, as alluded to above, that the bent configuration of X_3 is actually more probable than the linear configuration of X_3 even though the latter is a lower energy configuration in the LEPS potential. The effective potential "knows" about the entropy effect of having more bent configuration space available to compensate for the higher activation energy of the bent X_3 geometries.

The effective potential, $\Phi'(r_1,r_2,\theta)$, is used in the selection of the initial position and momentum coordinates for X_3. Normal modes are determined at the potential energy minimum of $\Phi'(r_1,r_2,\theta)$ which, as can be seen from Fig. 2, is well approximated by a quadratic potential close to the minimum in the saddle point region. These normal modes may be interpreted geometrically as a bending mode, a symmetric stretch mode, and an unstable asymmetric stretch mode which has imaginary frequency and is used to define the reaction coordinate. Eq. (2.11) is evaluated by selecting values of r_1, r_2, and θ using a Gauss-Hermite quadrature in the normal modes of Φ', as suggested by Eq. (2.20). The asymmetric stretch variable is constrained to be zero, thus defining the transition state surface upon which all trajectories start. (It is not even a good idea to evaluate the integral Eq. (2.18) by the above method using the unmodified potential, Φ^{LEPS}, due to the fact that the LEPS potential as a function of θ is poorly represented by a quadratic potential for which the normal mode analysis is applicable.)

As previously noted, the integration over the momentum variables, p in Eq. (2.17), is also performed using Gauss-Hermite quadrature in the normal modes, and the momentum quadrature in the asymmetric stretch is chosen to be even to ensure that there will always be some initial non-zero velocity along the reaction coordinate. (Choosing odd quadrature would give at least one initial condition for which the asymmetric stretch momentum is zero). For every selection of the initial conditions of X_3, the remaining slow position coordinates of the solvent are chosen by constraining the X_3 geometry at the minimum in $\Phi'(r_1,r_2,\theta)$ while allowing the solvent to equilibrate using molecular dynamics. This ensures that a significantly different solvent configuration is chosen for each trajectory in the ensemble. (Using MD in this manner to choose initial position and momentum coordinates for the solvent requires considerable computational effort.) Finally, the momentum variables of X_3, P, are selected by a Gaussian random number generator in a Boltzmann distribution at temperature 298 K.

3. Trajectories

Trajectories are produced, using the *full* Hamiltonian, by propagating both forward and backward in time from time zero at the initial conditions on the gas phase transition state surface. For trajectories which turn out to be reactive, propagating in one direction gives the dynamics from the transition state to products while propagating in the other direction gives the previous time history from reactants to the transition state. For unreactive trajectories, both forward and backward propagation leave the same atoms bonded together. One way to double the statistics in the evaluation of Eq. (2.11) without having to select twice as many solvent configurations is to run *two* trajectories for each solvent configuration, one trajectory with initially positive velocity and the other with initially negative velocity in the asymmetric stretch.

Finally, we have verified for the conditions presented here that there is *no* recrossing of this surface in the gas phase, so that TST is exact there.

III. X_3 in Argon

In this section we present our results for the special case of the hypothetical reaction of X + X_2 in liquid argon, with X having the mass of chlorine 35. The LEPS parameters are initially chosen to describe a 20 kcal/mol barrier height, a barrier frequency of 419 cm^{-1} and the isolated molecule Cl_2 Morse potential[36] (see Table 2). The Lennard-Jones parameters (see Table 1) characterize a weakly-interacting solvent which consists of 100 argon atoms at a density of 1400 kg m^{-3} ($\rho\sigma^3 = 0.83$) designed to approximate the density of argon when cool enough to liquefy at a pressure of 1 atmosphere. (The actual molecular dynamics are carried out at 298 K.) Results for this system described in Sec. A are then analyzed in Sec. B, while the effects of lowering the barrier frequency are considered in Sec. C.

A. Results

According to simple TST, every trajectory which arrives at the transition barrier goes directly on to form products. We examine this assumption for the 20 kcal/mol X_3 in argon system and observe that there are *no* solvent induced barrier recrossings in the 126 trajectories sampled; TST is exact. The reasons for this are described below in Sec. B.

There is, however, a considerable effect of the solvent on the *details* of the reaction trajectories as they approach to, and recede from the transition barrier. Figure 3 illustrates how the solvent can perturb a typical reactive trajectory by comparing the trajectory on the gas phase potential surface and in solution. The solvent is seen to change the precise course of the trajectory away from the barrier compared to its unperturbed path in the gas phase. This process can be understood in simple terms by examining the time-dependent exchange of energy between the various active degrees of freedom of X_3 and the solvent. Using Eq. (2.11), the average energy of X_3 as a function of time during the reaction is computed for 126 trajectories. After the center of mass motion of X_3 is removed, the average total energy of X_3 is partitioned into the modes of X_2 vibration, rotation and translation and the translational energy of the X atom. This partitioning is not uniquely definable in the sense that other definitions are possible, reflecting the lack of chemical precision in defining reactants and products in the transition barrier region because of the strong X_3 interaction there. We choose to conveniently define the two closest X

atoms as being "diatomic" X_2 and the other atom as being "free". When one atom becomes well separated from the other two this definition becomes chemically meaningful and the LEPS potential reduces to just the bound X_2 Morse potential. The total "vibrational" energy is then taken to be the sum of the vibrational kinetic energy of the closest two atoms and the *total* LEPS potential energy of all three atoms. (There is, of course, exchange of vibrational energy with the solvent.) Note that the zero of the LEPS potential function is taken to be the potential energy of an isolated X_2 molecule at its equilibrium geometry.

Figure 4 shows the average over 126 trajectories, illustrating the time-dependent partitioning of energy for X_3 in argon solvent (solid line) at T = 298 K, and compares this with the average X_3 partioning as a function of time in the gas phase (filled circles). Time zero is at the transition barrier. The plot is symmetrical about time zero as a consequence of the symmetry in the potential function. It is observed that there is a short period of time before and after the transition barrier, between approximately -0.05 ps to 0.05 ps, for which the partitioning of energy of the X_3 in solution is *just like that in the gas phase*, in accord with the representative trajectory shown in Fig. 3. At longer times away from the transition barrier, relaxation of the X_2 translational and rotational energy and the X atom translational energy in the solvent reduces the average total energy of the X_3 system by approximately 17 kcal/mol relative to the initial total energy at the transition barrier. No such decay can occur in the gas phase where the total X_3 energy must of course remain constant. The X and X_2 excess translational energy increases sharply as one falls from the transition barrier, reaching a plateau in the gas phase but rapidly decaying in solution as energy is transferred to the solvent. These processes have an approximately 0.2 ps time scale. Similar effects can be seen in the X_2 rotational energy with a time scale of about 0.2 ps. This rotational energy is small, originating[43] from a) the repulsion of the X from the X_2 for bent original configurations, b) bend vibrational motion at the barrier, and c) the original angular momentum of the X_3 at the transition barrier.

The energy in the separated diatomic X_2 vibration decays in approximately 0.25 ps to about 3 $\hbar\omega$, where ω is the ground state angular vibration frequency, 560 cm^{-1}, of $X_2 = Cl_2$, thus making the product diatomic vibrationally "hot" for a comparatively long period even in solution. This feature is shown by Fig. 4 to be identical in both phases and thus is governed exclusively by the LEPS potential of the reaction system. One expects there to be residual vibrational energy in part because the X-X bonds at the transition barrier are slightly longer than the equilibrium X_2 bond length. This excess vibrational energy does *not* relax significantly into the argon solvent in a 1.0 ps interval (Fig. 4), but rather over a time period measuring hundreds of picoseconds. This was verified by integrating one typical trajectory out to 250 ps and observing that the vibrational energy decays over this time period to about half of its "initial" value of 3 $\hbar\omega$.

For this system, the reaction outcome is determined on a *very short* time scale. The characteristic time scale for the reaction fate to be decided is less than 0.1 ps and the reaction *per se* is essentially finished after the rotational and translational energy is dissipated to the solvent. We explore this aspect further by considering the space and time dimensions within which the reaction probability is sensitive to solvent momentum perturbation using a method suggested by Andersen.[29] An ensemble of eighty reactive trajectories with the 20 kcal/mol barrier in argon solvent is selected, and the trajectories are interrupted at some time, τ, before crossing the barrier; all solvent molecules outside a sphere of a given radius measured from the center of mass of X_3 are given random momenta selected from a Boltzmann distribution while keeping all position coordinates the same. Note that the momenta of the reactive trajectories is *not* necessarily Boltzmann. The ability of such a solvent momentum perturbed trajectory to cross the barrier is a measure of the solvent momentum "sphere of influence" in time and space upon the reaction. Figure 5 shows a 3D plot of the probability of successful reaction versus both the time, τ, between momentum perturbation and original trajectory barrier crossing, and the radius of the spatial sphere outside which the solvent momentum is perturbed. We find, as one might intuitively expect, that for a constant spatial radius, the probability of reaction decreases for increasing time while, for constant time, the probability of reaction increases for increasing radius. If all of the solvent molecules' momenta are perturbed (*i.e.* for radius set equal to zero) at time τ, then it is seen that for τ > 0.14 ps the solvent is able to divert all trajectories away from reaction. Note that this 100% diversion time is on the same time scale as the fastest energy relaxation process, *i.e.* translational energy relaxation; this is also as one would expect on the basis of Fig. 4. The perturbation in solvent momenta must

evolve by translation into a perturbation in solvent positions before the force imparted to the X_3 by the solvent is altered, and thus finally the motion of the X_3 over the barrier can be deflected.

B. Discussion and Analysis

1. Recrossings

We observe no solvent induced recrossings for 126 trajectories with the X_3 system in argon with the 20 kcal/mol barrier. This can be easily understood qualitatively by realizing that the characteristic time scale[16,18] on a barrier of frequency ω_b = 419 cm^{-1} is on the order of $(\omega_b)^{-1}$ = 0.01 ps. On this sharp energy barrier, the fate of the trajectory is decided very quickly (~ 0.01 ps) and there is essentially no time for the solvent to influence the outcome of the reaction through any effective collisions with the X_3. This idea of the solvent motion and its effect on the reaction dynamics can be expressed more quantitatively by relating the time dependent solvent friction acting on the reaction coordinate[16,17] to the transmission coefficient κ

$$\kappa = \frac{k}{k^{TST}} \ . \tag{3.1}$$

The time dependent friction, $\zeta(t)$, is given by the time correlation function of the fluctuating forces on the reaction coordinate

$$\zeta(t) = (\beta/\mu) \langle F F(t) \rangle \ , \tag{3.2}$$

in which F is the force acting on the reaction coordinate with effective mass μ and $\beta = (k_B T)^{-1}$. This friction, plotted in Fig 6, is computed by freezing the X_3 coordinates with a bent X-X-X geometry corresponding to the minimum in potential energy of the effective potential, $\Phi'(r_1,r_2,\theta)$ (see Sec. II and Fig. 2), on the transition barrier, and measuring the time correlation function of the fluctuating solvent forces resolved onto the reaction coordinate.[17] The time dependent friction is also computed for the X_3 species in the linear geometry on the transition barrier and is illustrated in Fig. 7. This friction is similar to that for the bent geometry, which demonstrates that the bend angle of X-X-X at the transition state does not significantly affect the nature of the time dependent friction. Because of the very fast passage over the barrier, the effective friction acting on the reaction coordinate is not the full time integrated friction ζ given by Eq. (1.2), but is rather closer to the "instantaneous friction" felt by the reaction system. A convenient approximate measure of this is the value of the friction at time zero

$$\zeta(t = 0) = (\beta/\mu) \langle F^2 \rangle \equiv \omega_\zeta^2 \ , \tag{3.3}$$

which we describe in terms of an initial frictional frequency, ω_ζ. In contrast, the full friction, ζ, would be important for long time scale (e.g., diffusion controlled) processes. In Fig. 6 we see that the solvent friction for argon acting on the bent X_3 system falls off in an approximately "Gaussian" manner with a characteristic time τ = 0.19 ps from its initially weak (ω_ζ = 35 cm^{-1}) value; in particular, ω_ζ is small compared to the barrier frequency, ω_b, value of 419 cm^{-1}. Since $\omega_\zeta / \omega_b << 1$ we would expect,[16-18] as we indeed observe in the dynamics, that there are no solvent induced recrossings (in 126 trajectories), that κ is very close to one, and thus that TST is valid. This result will also hold for the linear geometry for which the initial value of the friction and the short time "Gaussian" decay is the same as for the friction of the bent geometry (see Fig. 7). (However, the time decay of the friction is slightly longer for the linear geometry than for the bent geometry. Thus, for the short time scale barrier crossing, the linear and bent X_3 system experiences the same friction, but for longer time scale processes, the linear system would have slightly more friction than the bent system.)

The time dependent friction on the reaction coordinate is explicitly incorporated into the generalized Langevin equation theory of Grote and Hynes[16-18] for rate processes. Here, κ is calculated as

$$\kappa = \lambda_r / \omega_b \ , \tag{3.4}$$

in which λ_r is termed the reactive frequency and is a measure of the solvent response to the reactive motion across a barrier of frequency ω_b. It is determined from the self-consistent equation

$$\lambda_r = \frac{\omega_b^2}{\lambda_r + \zeta(\lambda_r)} \ , \tag{3.5}$$

which involves the barrier frequency, ω_b, and the Laplace transform frequency component of the time dependent friction

$$\zeta(\lambda_r) = \int_0^\infty dt\, e^{-\lambda_r t}\, \zeta(t) \tag{3.6}$$

at the reactive frequency λ_r. For very small friction Eqs. (3.4) and (3.5) give $\lambda_r \approx \omega_b$ and $\kappa \approx 1$. Also, for sharp barriers, it can be shown[16-18] that $\lambda_r \approx \omega_b$ and, again, $\kappa \approx 1$. If we consider stronger friction or more rounded barriers, then it is expected that κ will decrease and that there will be barrier recrossings. With a Gaussian approximation to the decay time behavior of $\zeta(t)$ (Fig. 6),

$$\zeta(t) = \omega_\zeta^2\, e^{-(t/\tau)^2} \tag{3.7}$$

and use of Eqs. (3.4), (3.5) and (3.6), κ can be simply determined as a function of barrier frequency ω_b for various values of ζ and the results are shown in Fig. 8. The calculation for argon with ω_b = 419 cm^{-1}, ω_ζ = 35 cm^{-1}, and the relaxation time τ = 0.19 ps, given by fitting Eq. (3.7) to the data in Fig. 6, gives κ = 1.0, in agreement with the results from the molecular dynamics computation.

These results emphasize that it is the solvent response at the reactive frequency which determines how effective the solvent is in hindering the reaction progress over the barrier. The friction felt by the reaction system during the time period $(\omega_b)^{-1}$ is likely much smaller than the long time friction ζ. Thus, it is not surprising that the 20 kcal/mol barrier reaction of X_3 in argon solvent, which spends little time on the barrier, exhibits very few recrossings and κ = 1. Fig. 8 also shows that for smaller values of ω_b, κ is predicted to eventually decrease, and simple TST to ultimately fail. We explore the effect of lowering the barrier frequency, ω_b, in Sec. C and will see that, for lower barrier frequencies, the effect of the solvent friction increases and some recrossings are observed.

2. Energy Relaxation

The observed basic patterns of energy relaxation in Fig. 4 are what we intuitively expect, $\tau_{TRANS} \approx \tau_{ROT} \ll \tau_{VIB}$, and can largely be understood in terms of existing models of energy and phase decay.[44-47] Vibrational energy relaxation by the solvent is much slower than translational and rotational energy decay and this is understood by considering that the effective friction at the oscillator frequency,

$$\zeta_d(\omega_{osc}) = \int_{-\infty}^{\infty} dt\, e^{i\omega_{osc} t}\, \zeta_d(t)\,, \tag{3.8}$$

estimated by a Landau-Teller type expression is very small due to the high X_2 oscillator frequency of approximately 560 cm^{-1}. The "d" subscript emphasizes that the time dependent friction here refers to the correlation of the solvent forces on the diatomic fragment.

Since the remaining 3 $\hbar\omega$ vibrational energy in the nascent product X_2 decays only slowly and the corresponding amount in the nascent reactant X_2 is only acquired slowly, a natural question arises: Is vibrational activation up to $E_V = 3\,\hbar\omega$ of the reactants the rate limiting step? If so then the rate constant, k, will depend upon the *dynamics* of vibrational activation by the solvent. The answer is no. This can be explained with the aid of the Stable States Picture of reactions.[10,18,48] For a symmetric reaction the influence of the vibrational activation up to energy E_V is

$$k = \frac{k^{TST}}{1 + 2k^{TST}/k_V}\,, \tag{3.9}$$

in which the influence of the solvent on the barrier passage is justifiably ignored and k_V is the vibrational activation rate constant up to E_V. The structure of k_V is

$$k_V = Z_V\, e^{-\beta E_V}\,, \tag{3.10}$$

where Z_V refers to the details of the vibrational activation process, *e.g.*, Landau-Teller type transitions. Clearly vibrational activation dynamics are only rate limiting if they represent the slow step: $k_V \ll k^{TST}$. But since E_V is approximately 5 kcal/mol while the activation energy is 20 kcal/mol, we instead have $k^{TST} \propto e^{-\beta E^\ddagger} \ll k_V$. Thus the barrier passage is rate limiting, $k \to k^{TST}$ and the dynamics of vibrational energy transfer to and from the solvent play no role in the reaction rate. (The relative unimportance of

vibrational energy transfer in atom transfer as opposed to isomerizations has been discussed[10] elsewhere). Not only must the X_2 be properly vibrationally excited, but also the liquid must be in a part of phase space where it can translationally (and rotationally) thrust the X atom and the X_2 molecule together with sufficient energy to reach the barrier top. The TST rate constant reflects the equilibrium probability of all of these events occurring simultaneously.

Finally, it is conceivable that the approximately 17 kcal/mol of energy rapidly transferred to the solvent in the reaction could have resulted in a local "heating" effect, in which translationally energized solvent atoms quickly reactivate the incipient products to recross the barrier. This does not occur; instead the excess energy is rapidly transferred to the other solvent atoms outward from the site of the reaction.

3. Simple Model for Reaction

A simple 3-stage picture for this reaction, as shown in Fig. 9 emerges in light of the above observations: activation of reactants in stage 1, barrier crossing in stage 2, and deactivation of products in stage 3. In the first stage the dynamical role of the solvent is to furnish activation energy to the reactants and properly phase their motion in a fashion analogous to the way it absorbs the excess energy and dephases the products formed in stage 3. There are three time scales for energy exchange with the solvent in the first and third stages corresponding to vibrational, rotational and translational energy exchange. In addition to solvent induced energy activation and relaxation (t_1), the reaction also requires the proper phasing among relative translational, rotational and vibrational motions (t_2). The second stage includes formation from the energized reacting species of the activated complex and barrier crossing. Here, for $\omega_b >> \omega_t$, the reaction proceeds over the barrier top largely unimpeded by the solvent, and recrossings are not observed. In Fig. 4 one can see that the partitioning in the liquid and gas phases is essentially the same for a time period of about -0.05 ps to 0.05 ps. In this period the weakly-interacting solvent simply does not have enough time to interfere with the reaction progress, and there is essentially unimpeded gas phase dynamics for the crossing over the barrier. This statement holds even though, as shown in Fig. 3, for longer times before and after the transition barrier the reaction in the liquid phase bears little resemblance to a gas phase reaction. As soon as the incipient products are formed in stage 3 they rapidly transfer translational and rotational energy back to the solvent, and are thus energetically prohibited from recrossing the barrier. The opposite situation, whereby the solvent transfers additional energy to the products after they are formed, is not observed because, as discussed in Sec. III.B.2, the energy of the products is high compared to k_BT and the more probable event is energy deactivation. Thus, we find TST to be an excellent description for this reaction.

We now examine the effect on the dynamics and the rate constant of lowering the barrier frequency.

C. Variation of Barrier

In Sec. III.A we found that TST is appropriately and successfully applied in the region -0.05 ps to 0.05 ps during which time the barrier is crossed and the fate of each trajectory is decided. We find, as predicted,[16,18] that TST is valid for the case of a sharp barrier and a weakly-interacting solvent. But if the barrier frequency is lowered sufficiently, then the characteristic time, $(\omega_b)^{-1}$, on the barrier may become sufficiently long that the solvent has time to induce recrossings (see Fig. 8); then it is predicted that TST should fail to some extent ($\kappa < 1$)

Since we are concerned with the solvent's ability to disrupt motion across the barrier and the subsequent breakdown of TST, we will consider the effect of changing the barrier frequency, ω_b, as motivated above. A simple modification of the LEPS potential parameters ${}^3D_i$, i = 1,2,3 (see Table 2), allows the simultaneous adjustment of the barrier height and barrier frequency, while preserving the asymptotic characteristics. The barrier height has no *direct* bearing on the dynamical influence of the solvent although it will affect the probability of formation of the activated complex (and hence the rate constant) through the Boltzmann weighting $e^{-E^{\ddagger}/k_BT}$ where $E^{\ddagger}$ is the barrier height. All other things being equal, a lower barrier height will result in a lower barrier frequency. We select two additional barrier heights of 10 kcal/mol and 5 kcal/mol with corresponding barrier frequencies 288 cm^{-1} and 168 cm^{-1}, as shown in Table 2.

Trajectories are run on the above potential energy surfaces in argon solvent. While no recrossings occur for the 10 kcal/mol barrier, some recrossings are observed for the 5 kcal/mol barrier. A barrier crossing is counted each time that the value of the asymmetric stretch reaction coordinate changes sign during the course of the trajectory, beginning with an initial crossing toward either the product side or the reactant side. Crossing statistics for ensembles of trajectories are presented for the 20 , 10 and 5 kcal/mol barriers in Tables 3a, 3b and 3c respectively. The statistics in the tables are determined by computing trajectories initialized at the transition barrier with either positive (toward products) or negative (toward reactants) momentum in the asymmetric stretch reaction coordinate. The table shows that some recrossings occur for the lowest barrier reaction.

Table 3 (a). Barrier Crossings for 20 kcal/mol X_3 Barrier in Argon

Number of Crossings	Initial and Final States of Trajectories			
	Reactant - Reactant	Reactant - Product	Product - Reactant	Product - Product
1	0	126	126	0

Table 3 (b). Barrier Crossings for 10 kcal/mol X_3 Barrier in Argon

Number of Crossings	Initial and Final States of Trajectories			
	Reactant - Reactant	Reactant - Product	Product - Reactant	Product - Product
1	0	32	32	0

Table 3 (c). Barrier Crossings for 5 kcal/mol X_3 Barrier in Argon

Number of Crossings	Initial and Final States of Trajectories			
	Reactant - Reactant	Reactant - Product	Product - Reactant	Product - Product
1	0	27	26	0
2	5	0	0	4
3	0	0	2	0

Thus, Table 3c indicates that while 27 trajectories with initially positive momentum directly formed products, 5 trajectories recrossed quickly to form reactants. Similar features are displayed for trajectories with initially negative momentum. However, the crossing patterns in the table report only the number of trajectories for a particular number of crossings and give little indication of the relative *probabilities* for those trajectories determined by the quadrature discussed in Section II.C. One estimate of the importance of these probabilities is to compute the average number of crossings with proper weightings using Eq. (2.11) for only those trajectories which react. For the 20 kcal/mol, 10 kcal/mol and 5 kcal/mol barriers the average number of crossings is 1.00, 1.00 and 1.03 respectively. A better estimate for the recrossing influence on the rate constant is the transmission coefficient κ.

The effect of the recrossings is to make TST an overestimate of the rate constant, and the correction to the TST rate constant is given by $\kappa \leq 1$. We will determine the correction κ, rather than the rate constant k itself, as the latter requires a knowledge of the free energy of activation due to solvent effects, *i.e.* the potential of mean force, which is a computationally intensive calculation using MD.[49-51] Furthermore, κ is a direct measurement of the dynamical influence of the solvent in affecting the rate

constant.

1. Expression for κ

According to the Stable States Picture of reactions[48] the rate constant, k, can be expressed by the correlation function formula

$$k = \int_0^\infty dt \, \langle \, j \, j^*(t) \, \rangle_R \, , \tag{3.11}$$

in which j is the flux counted positive from reactants across the transition barrier at time zero and $j^*(t)$ is the flux counted negative toward products at a later time t. The asterisk indicates that the dynamics of the trajectory must be followed only long enough that either a stable reactant or product is formed (this typically occurs in our reaction system in much less than 1.0 ps) and $\langle \, \rangle_R$ denotes an average over the equilibrium distribution, normalized by the reactant partition function Q_R. The time integral adds up all the reactive flux into stable products so that the more reactive trajectories there are, the larger is the correlation and the larger is the rate constant k. The expression for k in Eq. (3.11) is equivalently written upon integration as[10]

$$k = \lim \langle \, j \, \theta[x(t)] \, \rangle_R \, , \tag{3.12}$$

where the limit means we follow trajectories only long enough in time to determine whether they form stable products or reactants, $\theta[x(t)]$ is a step function which equals one on the product side and zero on the reactant side and $x(t)$ is the asymmetric stretch reaction coordinate as a function of time such that x is zero at the transition barrier for $t = 0$. We now describe various calculational forms of Eq. (3.12) which are convenient for calculating the transmission coefficient κ and closely related to the observed crossing patterns displayed in Table 3.

In simple TST, the rate constant can be calculated by assuming that every trajectory at the transition barrier which has initial positive flux toward products will always end up as products, while such trajectories with initial negative flux toward reactants will always go to reactants. Only those trajectories which form products contribute to the simple TST rate constant, and there are never any recrossings. Thus, in calculating k^{TST}, we need to consider only those trajectories which have initially positive flux, j_+, and there is no need to follow dynamics for any time past zero because the fate of all trajectories is decided by sign of their initial momenta. The flux j_+ is given by the velocity across the transition barrier, $(p/\mu)\,\delta(x)$, where p is momentum, μ is the reduced mass along the reaction coordinate of the X_3 species, $\delta(x)$ is the delta function of position along the reaction coordinate with $x = 0$ at the barrier, and the TST rate constant is[4,6,20,21,39,52]

$$\begin{aligned} k^{TST} &= \langle \, j_+ \, \rangle_R \\ &= \langle \, (p/\mu) \, \delta(x) \, \theta[x(t)] \, \rangle_R \\ &= \langle \, (p/\mu) \, \theta(p) \, \rangle_R^{\ddagger} \, , \end{aligned} \tag{3.13}$$

in which ‡ indicates that we need to consider only the initial conditions at the transition barrier, and $\theta(p)$ is a step function which is one for positive momenta at the transition barrier and zero for negative momenta.

In the presence of recrossings, the actual rate constant, Eq. (3.12), is conveniently split into two parts representing contributions from the trajectories with initially positive momentum and those with initially negative momentum as

$$k = \langle \, j \, \theta[x(t)] \, \rangle_R = \langle \, j_+ \, \theta[x(t)] \, \rangle_R + \langle \, j_- \, \theta[x(t)] \, \rangle_R \equiv k_+ + k_- \, , \tag{3.14}$$

in which j_+ represents the initially positive flux while j_- is the initially negative flux across the transition barrier, both determined by the magnitude and direction of the initial velocities along the asymmetric stretch reaction coordinate at the transition barrier. We have three methods of applying Eq. (3.14) to the calculation of the transmission coefficient for the rate constant using MD.

Method 1 is to sample trajectories which always have initially *positive* velocities at the transition barrier at time zero. This focuses, as does TST, on those trajectories initially headed toward products

from reactants. For the contribution k_+, the fate of the trajectories is determined by computing the dynamics forward in time. For the contribution k_-, we imagine time reversing the velocities of all particles in the reaction system. This time reversal converts j_- to $-j_+$ in the k_- contribution to k in Eq. (3.14) as well as changing the sign of t in $\langle\, j_- \,\theta[x(t)]\,\rangle_R$. Thus k_- is given by

$$\langle\, j_- \,\theta[x(t)]\,\rangle_R = -\langle\, j_+ \,\theta[x(-t)]\,\rangle_R \,. \tag{3.15}$$

The step function $\theta[x(-t)]$ indicates that the trajectories must originate from the *products* side in the asymptotic past. Thus, the total rate constant is given in terms of initial positive velocity trajectories by

$$k = \langle\, j_+ \,\theta[x(t)]\,\rangle_R - \langle\, j_+ \,\theta[x(-t)]\,\rangle_R \,, \tag{3.16}$$

and the transmission coefficient κ is

$$\kappa = \frac{k}{k^{TST}} = \frac{\langle\, j_+ \,\theta[x(t)]\,\rangle_R - \langle\, j_+ \,\theta[x(-t)]\,\rangle_R}{\langle\, j_+ \,\rangle_R} \,. \tag{3.17}$$

Figure 10 illustrates the three predominant types of crossings observed (Table 3): (a) is a direct, successful reactant → product transition with no recrossing; (b) is a single recrossing, reactant → product → reactant, after the transition barrier is initially crossed in the forward direction, and (c) is a single recrossing, product → reactant → product, in which the recrossing occurs prior to a reactant → product crossing at $t = 0$. The equilibrium distribution on the transition barrier is determined by the algorithm for sampling the initial conditions using Eq. (2.11), in which the unnormalized probability $w_i = e^{-H(q,p,R,P)/k_BT}$ and the initial velocities v_i along the asymmetric stretch, are determined for each trajectory i in the ensemble average. Thus, for N trajectories in the ensemble average, κ is computed as

$$\kappa = \frac{\sum_{i,+}^{N} w_i \,|v_i| \, Q_i}{\sum_{i,+}^{N} w_i \,|v_i|} \,, \tag{3.18}$$

where + indicates all trajectories have initially positive velocity across the transition barrier, and the value of Q_i depends on the initial and final states of the trajectory i,

$$Q_i = \begin{cases} +1 & \text{if Reactant} \rightarrow \text{Product} \\ 0 & \text{if Reactant} \rightarrow \text{Reactant or Product} \rightarrow \text{Product} \\ -1 & \text{if Product} \rightarrow \text{Reactant} \end{cases} . \tag{3.19}$$

As described in Sec. II.C.2, before a particular trajectory is computed, the X_3 coordinates are constrained while solvent coordinates are randomized by integrating the solvent dynamics out to many picoseconds. This ensures that a significantly different solvent configuration is chosen for each trajectory in the ensemble. Using MD in this manner to choose initial position and momentum coordinates for the solvent requires considerable computational effort. One way to double the statistics in the determination of κ without having to select twice as many solvent configurations is to run *two* trajectories for each solvent configuration, one trajectory with initially positive velocity and the other with initially negative velocity in the asymmetric stretch. This is method 2 for calculating κ, in which the trajectories are sampled with both positive and negative initial asymmetric stretch velocities and time reversal is applied to all trajectories in order to compute the dynamics and determine the initial and final states. The negative flux initial conditions are chosen from the positive flux initial conditions by just changing the sign of the velocities of the X_3 while keeping all position coordinates and the solvent's velocities unchanged. Thus, the total number of sampled trajectories is twice that in method 1 and there is an equal number of sampled trajectories from both the positive and negative flux initial conditions with corresponding equal weights, w_i, and equal but opposite velocities, v_i, for X_3. Since the reaction is symmetric with respect to reactants and products, the definition of reactants and products is a matter of convention for a given trajectory. In method 2, as in method 1, we want to sample *all* trajectories which are headed initially towards reactants, so the definition of reactants and products will depend on whether the flux is positive or negative. In method 2, all positive flux initial conditions (also used in

method 1) are defined as heading toward products, while all of the negative flux initial conditions are also counted as heading toward products for the TST prediction (only for method 2). This gives κ as

$$\kappa = \left[\sum_{i,\pm}^{N} w_i |v_i|\right]^{-1} \left[\sum_{i,+}^{N} w_i |v_i| Q_i - \sum_{i,-}^{N} w_i |v_i| Q_i\right], \tag{3.20}$$

where $\pm$ indicates all trajectories with either positive or negative flux, + indicates trajectories with positive flux only and – indicates trajectories with negative flux only. Eq. (3.20) can be shown to follow directly from Eq. (3.19).

Finally, in method 3, we use the positive and negative flux distributions as described in method 2 but keep the definition of reactants and products the same for both the positive and negative flux initial conditions. This convention corresponds to the definition of reactants and products in Table 3. Thus, all positive flux initial conditions are headed toward products, and all negative flux initial conditions are headed toward reactants. Only knowledge of the final outcome of the reaction and the magnitude and direction of the initial flux is required to compute the transmission coefficient. Trajectories which end up as products contribute either positively or negatively to the rate constant according to whether their initial flux is positive or negative. This leads to the expression

$$\kappa = \left[\sum_{i,+}^{N} w_i |v_i|\right]^{-1} \left[\sum_{i,+}^{N} w_i |v_i| Q'_i - \sum_{i,-}^{N} w_i |v_i| Q'_i\right], \tag{3.21}$$

where

$$Q'_i = \begin{cases} 1 & \text{if Product} \\ 0 & \text{if Reactant} \end{cases}. \tag{3.22}$$

This last formula is the direct implementation of Eq. (3.14) when divided by k^{TST}. It is also related to that developed by Chandler[53] and employed in isomerization studies.[54] It differs in that trajectories here are simply followed until stable reactants or products are formed, rather than until certain correlations plateau in time.[53,54]

All three methods will give the same answer in the limit of an infinite number of sampled trajectories, but methods 2 and 3 are ways to maximize the available computer time by doubling the number of sampled trajectories without having to recompute a new set of initial solvent configurations. Methods 2 and 3 require only a small additional amount of computer time compared to method 1.

2. Results for κ

For the 5 kcal/mol barrier with a barrier frequency of 168 cm^{-1}, κ is computed from an ensemble of 64 MD trajectories and using methods 1, 2 and 3 as 0.91, 0.92 and 0.91 respectively. Using Eq. (3.4) and a Gaussian approximation to the time dependent friction for argon given by Eq. (3.7) with τ = 0.19 ps, κ is determined from Grote-Hynes theory as 0.98 for the 5 kcal/mol barrier. For the 10 kcal/mol barrier (and the 20 kcal/mol barrier), both MD and Grote-Hynes theory predict κ to be one. These calculations are compared in Table 6. The agreement in the full MD and time dependent friction methods of calculating κ is excellent, and both methods give the lowest value of κ for the lowest barrier frequency.

It is clearly very interesting to go to lower barriers with lower ω_b values, and we have examined a 2.6 kcal/mol barrier which has a barrier frequency of ω_b = 20 cm^{-1}. However, for this barrier we find multiple recrossings in the *gas* phase. These apparently arise from intramolecular energy flow between the reaction coordinate and coupled non-reactive modes.[55] The longer time spent on the barrier, $(\omega_b)^{-1}$ = 0.3 ps, may allow such coupling effects to develop. These isolated molecule dynamics must be understood before the solvent influence on the reaction can be properly characterized, and this topic is left for future research. Nonetheless it is worth stressing this observation as a cautionary example of the possible unphysical character of low-barrier, one-dimensional reaction studies which ignore other internal degrees of freedom.

3. Energy Relaxation

The energy decay patterns for X_3 in argon for the 10 kcal/mol and 5 kcal/mol barriers are similar to those for the 20 kcal/mol barrier in Fig. 4 but are scaled down in magnitude in proportion to the barrier heights. The energy decay patterns are presented for the 5 kcal/mol barrier in Fig. 11. An interesting new feature is the transient rise in solution of the potential energy plus diatomic vibrational kinetic energy of X_2 above the gas phase value. We have traced this to a certain "cage" effect in which the high density argon solvent temporarily holds the diatomic fragment in a region of finite X_3 potential energy.

IV. Variation of Solvent

In Sec. III above, calculations of energy decay, solvent momentum sphere of influence, recrossings, and κ were presented for the reaction $X + X_2$ in argon solvent. In this section we briefly explore the corresponding results in helium and xenon solvents. These represent "light" and "heavy" molecule solvents when viewed on the mass scale of X = Cl.

The solvent systems consist of 100 atoms at densities of 147 kg m^{-3} ($\rho\sigma^3 = 0.36$) and 3520 kg m^{-3} ($\rho\sigma^3 = 0.80$) for helium and xenon respectively, designed to represent the density of these solvents at a temperature cool enough to liquefy at a pressure of 1 atmosphere. The actual molecular dynamics are computed for a temperature of 298 K.

A. Energy Relaxation

The patterns for energy relaxation are shown in Figs. 12 and 13 for the 20 kcal/mol energy barrier in helium and xenon respectively. The corresponding results for argon are shown in Fig. 4. The translational and rotational energy decay times are faster in argon and xenon solvents and slower in helium solvent. Helium, with a small mass, should be less effective in exchanging these types of energy through collisions with X and X_2, and indeed energy decay to and from translational and rotational motion is relatively slow. Xenon, with a large mass, is similar to argon in its ability to dissipate the excess translational and rotational energy. These patterns are not unexpected. Although this is not shown in the figure, only helium begins to relax vibrational energy in less than 10 ps. This is in rough accord with a Landau-Teller picture in which high frequency force components arising from rapid helium motions are important.

As with argon, the energy decay patterns for lower barrier heights are similar to those for the 20 kcal/mol barrier but scaled down in magnitude. The energy relaxations for the 5 kcal/mol barrier in helium and xenon solvents are illustrated in Figs. 14 and 15 respectively. The cage effect discussed in Sec. IV.C.3 for the transient excess of X_3 potential plus diatomic vibrational kinetic energy for the 5 kcal/mol barrier in argon appears again in Fig. 15 for the high-density, heavy solvent xenon, but is absent in Fig. 14 for the lower density, light solvent helium.

Finally, the solvent momentum sphere-of-influence for the 20 kcal/mol barrier in helium solvent is shown in Fig. 16. The momentum effect on the reaction by helium solvent is lower in magnitude than for argon in Fig 5.

B. Recrossings

Trajectories are analyzed for recrossing patterns and the results for the 20, 10 and 5 kcal/mol energy barriers in helium and xenon solvents are presented in tables 4a, 4b, 4c, 5a, 5b, and 5c. There are no recrossings observed for the 20 kcal/mol and 10 kcal/mol barriers in *any* of the three solvents. Also note that there are no recrossings observed on any of the barriers in the absence of solvent (*i.e.* in the gas phase). The average number of crossings is computed for the 5 kcal/mol barrier in helium and xenon as 1.00 and 1.01, respectively. This average includes the relative weights of the trajectories.

In Sec. III we used the idea of the time dependent solvent friction acting on the reaction coordinate and found that, for the 20 kcal/mol barrier, the initial frictional frequency ω_ζ in argon solvent is much weaker than the frequency associated with the forces driving the reaction down the barrier, that recrossing are accordingly rare, and that the transmission coefficient $\kappa = 1$. For the low, 5 kcal/mol barrier height and frequency, some recrossings are observed and κ decreases slightly. The two

Table 4 (a). Barrier Crossings for 20 kcal/mol X_3 Barrier in Helium				
Number of Crossings	Initial and Final States of Trajectories			
	Reactant - Reactant	Reactant - Product	Product - Reactant	Product - Product
1	0	32	32	0

Table 4 (b). Barrier Crossings for 10 kcal/mol X_3 Barrier in Helium				
Number of Crossings	Initial and Final States of Trajectories			
	Reactant - Reactant	Reactant - Product	Product - Reactant	Product - Product
1	0	32	32	0

Table 4 (c). Barrier Crossings for 5 kcal/mol X_3 Barrier in Helium				
Number of Crossings	Initial and Final States of Trajectories			
	Reactant - Reactant	Reactant - Product	Product - Reactant	Product - Product
1	0	30	31	0
2	1	0	0	2

additional solvents helium and xenon have a time dependent friction which differs from argon, as illustrated in Figs. 6 and 7. Helium has a weaker friction than argon with initial frequency $\omega_\zeta = 15$ cm^{-1}, and a short decay time τ of about 0.06 ps, while the xenon friction is stronger with $\omega_\zeta = 40$ cm^{-1} and decay time τ of 0.36 ps. We observe that recrossings in these solvents (see Tables 4 and 5) for the low barrier of 5 kcal/mol are similar to what is seen for the low barrier height in argon (see Table 3). There are however, compared to argon, fewer recrossings in helium but more recrossings in xenon. This is in accord with the calculation that there is less short time solvent friction for helium and greater short time friction for xenon in comparison to argon. None of the solvents presents a great enough friction on the reaction coordinate to induce recrossings for barrier heights of 10 and 20 kcal/mol, as summarized in Table 6.

Using methods 1, 2 and 3 as described in Sec. III, κ is computed for 64 trajectories on the 5 kcal/mol barrier in helium as 0.96, 0.97 and 0.98, respectively, while κ for 252 trajectories on the 5 kcal/mol reaction in xenon is 0.91, 0.91, and 0.92. As seen here and in Table 6, κ decreases for lower barrier heights and for stronger solvent time dependent frictions. This is compared with Grote-Hynes (GH) theory, Eqs. (3.4) - (3.6), for computing κ, when we use a Gaussian approximation to the time dependent friction. For helium with a 5 kcal/mol barrier, barrier frequency $\omega_b = 168$ cm^{-1} and $\tau = 0.06$ ps, GH theory gives κ as 0.99, while for xenon, with $\tau = 0.36$ ps, κ is predicted to be 0.95. A comparison of κ computed from MD and GH theory is presented for all of the barrier heights and solvents in Table 6. The estimated error in the values of κ from MD for the 5 kcal/mol barrier is ± 0.03. The values for κ from GH theory compare within 0.05 of the values determined by molecular dynamics simulation and the trend for κ to decrease with decreasing barrier frequency and increasing initial solvent frequency are the same for both GH theory and MD.

The 5 kcal/mol reaction in xenon is an interesting one with which to calculate the predictions of Kramers Theory.[19] Since the xenon time dependent friction is of significant magnitude and fairly long

Table 5 (a). Barrier Crossings for 20 kcal/mol X_3 Barrier in Xenon				
Number of Crossings	Initial and Final States of Trajectories			
	Reactant - Reactant	Reactant - Product	Product - Reactant	Product - Product
1	0	126	126	0

Table 5 (b). Barrier Crossings for 10 kcal/mol X_3 Barrier in Xenon				
Number of Crossings	Initial and Final States of Trajectories			
	Reactant - Reactant	Reactant - Product	Product - Reactant	Product - Product
1	0	32	32	0

Table 5 (c). Barrier Crossings for 5 kcal/mol X_3 Barrier in Xenon				
Number of Crossings	Initial and Final States of Trajectories			
	Reactant - Reactant	Reactant - Product	Product - Reactant	Product - Product
1	0	72	74	0
2	19	0	0	21
3	0	31	21	0
4	7	0	0	4
5	0	1	2	0

lifetime, (Figs. 6 and 7), the friction constant

$$\zeta = (\beta/\mu)\int_0^\infty dt \, \langle \, FF(t) \, \rangle \, , \tag{4.1}$$

is considerable. We numerically estimate from Figs. 6 and 7 that $\zeta = 105\ cm^{-1}$ for the bent X_3 configuration and $\zeta = 198\ cm^{-1}$ for the linear configuration. Then the Kramers transmission coefficients[19]

$$\kappa = \sqrt{1 + (\zeta/2\omega_b)^2} - (\zeta/2\omega_b) \tag{4.2}$$

are 0.74 and 0.59 for the bent and linear configurations. These are noticeably less than the MD results and the Grote-Hynes prediction, emphasizing again the importance of the *short* time scale solvent dynamics for the reaction problem.

This short time aspect can be finally stressed by completely *ignoring* the time dependence of the friction. Then $\zeta(\lambda_r)$ in Eq. (3.5) reduces to $\omega_\zeta^2 / \lambda_r$ and we obtain the short time, nonadiabatic prediction of GH theory[16-18]

$$\kappa = \sqrt{1 - (\omega_\zeta / \omega_b)^2} \tag{4.3}$$

solely in terms of the barrier frequency and the initial time dependent friction value. Equation (4.3) agrees to within 0.01 with the Gaussian friction GH κ values listed in Table 6 and is thus in very good agreement with the MD κ values.

Table 6. Transmission Coefficients for Various Barriers and Solvents					
Barrier Height (kcal/mol)	Barrier Frequency (cm^{-1})	Solvent	κ (Molecular Dynamics)	κ (Grote-Hynes Theory)	Average Number of Barrier Crossings
20	419	He	1.00	1.00	1.00
		Ar	1.00	1.00	1.00
		Xe	1.00	0.99	1.00
10	288	He	1.00	1.00	1.00
		Ar	1.00	0.99	1.00
		Xe	1.00	0.98	1.00
5	168	He	0.97	0.99	1.00
		Ar	0.91	0.98	1.03
		Xe	0.91	0.95	1.01

Finally, the three solvents, helium, argon and xenon, display weak coupling with the reaction coordinate. This is reflected in the lack of recrossings observed for the higher barriers and relatively few recrossings on the lowest barrier. A more strongly interacting solvent, which has a larger initial value of the friction, ω_ζ, would be expected to decrease κ. One way to increase the solvent-solute coupling strength is to modify the value of the X_3-solvent Lennard-Jones parameter, ε_{ij}. When the value of ε_{ij} for argon-X interactions is multiplied by a factor of 128 we find that the dynamics with the 20 kcal/mol are not significantly different than the dynamics for the unchanged solvent. The rate of energy exchange with this modified solvent is much faster, but the transition barrier dynamics are the same; there are no recrossings, and κ is one. If the solvent interaction parameters are modified in this manner the solvent becomes very "sticky" and stays roughly locked in a particular configuration. This slows down the solvent motion significantly, and barrier passage occurs for a solvent configuration which is essentially fixed. However, even for this major increase in the solvent-solute coupling strength, the dynamics on the barrier are still roughly approximated by gas phase barrier dynamics. Unfortunately, the "sticky" character of the solvent prevented us from obtaining reliably equilibrated transition barrier initial conditions sufficient to pursue this case quantitatively.

V. Conclusions

Molecular dynamics have been computed for the hypothetical reaction of $X + X_2 \rightarrow X_2 + X$ (the mass of X set to chlorine) in three different liquid density inert gas solvents, He, Ar, and Xe. We find that this reaction can be largely understood in terms of a simple model of 3 epochs: a) build up of the reactant energy and phase relationships needed for activation, b) barrier crossing, and c) decay of energy and phase of products. Epochs a) and c) can largely be understood in terms of existing models of phase and energy decay while b) can largely be understood in terms of gas phase A + BC barrier crossing dynamics, even for the lowest barriers we have examined.

We find no solvent induced recrossings and thus no deviation from TST for reactions with higher barriers and barrier frequencies. A very small deviation from gas phase barrier crossing dynamics and thus a slight breakdown of TST due to recrossings of the barrier is found upon lowering the barrier

frequency; the characteristic time spent at the top of the barrier becomes longer and somewhat more comparable to the time scale for solvent motion, and the effect of friction by the solvent on the reaction coordinate increases. The model of time dependent friction acting on the reaction coordinate is shown to be useful in understanding and quantitatively predicting the role of the solvent in affecting the dynamics of barrier crossing and therefore the rate constant.

Three methods for computing the transmission coefficient from molecular dynamics have been presented and the computed results compared to the predictions of the Grote-Hynes equations in which the initial time dependent friction is approximated by a Gaussian. The molecular dynamics and Grote-Hynes theory give values for the transmission coefficient, κ, which compare within 0.05 and give the same trends of decreasing κ with increasing solvent friction and decreasing barrier frequency.

We have discussed the very low reaction barrier (2.6 kcal/mol) case in only a cursory fashion here, due to the apparent involvement of intramolecular energy flow features in the isolated gas phase reaction, thereby clouding the role of the solvent. We hope to analyze this interesting case in detail in the future. Other interesting possibilities for future study include strongly interacting solvents involving, for example, hydrogen bonding to the reaction system.[56,57]

We have studied here only the symmetric reaction case. There are new dynamical aspects present in asymmetric reactions; for example, the role of reactant vibrational excitation in accelerating reactions.[7] It will be interesting to examine whether these features survive in solution. Our present results are already highly suggestive in this regard.

A major finding of this work is that TST typically provides an excellent description for the rates of simple atom transfers in weakly interacting solvents. This means, for example, that one can with confidence use the methods of modern *equilibrium* statistical mechanics to compute solution rate constants using TST for such reactions. In this connection it should also be stressed that in addition to the dynamical effects discussed here, within the TST description there can be important *equilibrium* solvent effects on atom transfer free energy barriers and thus on rate constants.[58] The present work suggests that when these are accounted for, one might reliably predict, for example, the pressure variation of a simple atom transfer rate from gas to liquid phase densities in inert rare gas solvents.

ACKNOWLEDGMENTS

We acknowledge the donors of the Petroleum Research Fund, administered by the American Chemical Society, for partial support of this research. We also thank the National Science Foundation (Chemistry), CHE 84-19830, and CHE 84-07491-02, and the Office of Naval Research (Chemistry) for supporting this work and Domenic P. Ali and especially Bradley J. Gertner for their help.

References

1. S. Glasstone, K. J. Laidler, and H. Eyring, *Theory of Rate Processes* (McGraw-Hill, New York, 1941).
2. I. W. M. Smith, in *Prog. Reaction Kinetics, Vol. 10*, edited by R. M. Levy (Butterworth, London, 1974) p. 1.
3. M. R. Levy, Prog. Reaction Kinetics 10, 1 (1979).
4. E. Wigner, Trans. Faraday Soc. 34, 29 (1938).
5. P. J. Kuntz, in *Dynamics of Molecular Collisions, Part B*, edited by W. H. Miller (Plenum Press, New York, N. Y., 1976) p. 53.
6. P. Pechukas, in *Dynamics of Molecular Collisions, Part B*, edited by W. H. Miller (Plenum Press, New York, 1977) p. 63.
7. J. C. Polanyi, Accts. Chem. Res. 5, 161 (1972).
8. D. G. Truhlar, W. L. Hase, and J. T. Hynes, J. Phys. Chem. 87, 2664 (1983).
9. J. P. Bergsma, P. M. Edelsten, B. J. Gertner, K. R. Huber, J. R. Reimers, K. R. Wilson, S. M. Wu, and J. T. Hynes, Chem. Phys. Lett. 123, 394 (1986).

10. J. T. Hynes, in *The Theory of Chemical Reaction Dynamics, Vol. IV*, edited by M. Baer (CRC Press, Boca Raton, FL, 1985) p. 171.
11. J. T. Hynes, in *Ann. Rev. Phys. Chem., Vol. 36*(Annual Reviews Inc., Palo Alto, CA, 1985) p. 573.
12. D. Chandler, J. Stat. Phys 42, 49 (1986).
13. G. R. Fleming, S. H. Courtney, and M. W. Balk, J. Stat. Phys. 42, 83 (1986).
14. P. Hänggi, J. Stat. Phys. 42, 105 (1986).
15. J. T. Hynes, J. Stat. Phys. 42, 149 (1986).
16. R. F. Grote, G. van der Zwan, and J. T. Hynes, J. Phys. Chem. 88, 4676 (1984).
17. R. F. Grote and J. T. Hynes, J. Chem. Phys. 75, 2191 (1981).
18. R. F. Grote and J. T. Hynes, J. Chem. Phys. 73, 2715 (1980).
19. H. A. Kramers, Physica (The Hague) 7, 284 (1940).
20. C. H. Bennett, in *Diffusion in Solids*, edited by J. J. Burton (Academic Press, New York, 1975) p. 73.
21. C. H. Bennett, in *Algorithms for Chemical Computations: ACS Symposium Series 46*, edited by R. E. Christofferson (American Chemical Society, Washington, D. C., 1977) p. 63.
22. R. O. Rosenberg, B. J. Berne, and D. Chandler, Chem. Phys. Lett. 75, 162 (1980).
23. P. Bado, P. H. Berens, J. P. Bergsma, S. B. Wilson, K. R. Wilson, and E. J. Heller, Picosecond Phenom. 23, 260 (1982).
24. P. Bado, P. H. Berens, J. P. Bergsma, M. H. Coladonato, C. G. Dupuy, P. M. Edelsten, J. D. Kahn, K. R. Wilson , and D. R. Fredkin, Laser Chem. 3, 231 (1983).
25. J. A. McCammon, Rpts. Prog. Phys. 47, 1 (1984).
26. J. A. McCammon and M. Karplus, Ann. Rev. Phys. Chem. 31, 29 (1980).
27. E. K. Grimmelman, J. C. Tully, and E. Helfand, J. Chem. Phys. 74, 5300 (1981).
28. D. Beeman, J. Comput. Phys. 20, 130 (1976).
29. W. C. Swope, H. C. Andersen, P. H. Berens, and K. R. Wilson, J. Chem. Phys. 76, 637 (1982).
30. R. W. Hockney and J. W. Eastwood, *Computer Simulation Using Particles* (McGraw-Hill Inc., New York, N. Y., 1981).
31. D. J. Adams, in *The Problem of Long-Range Forces in the Computer Simulation of Condensed Media*, edited by D. Ceperly (National Resource for Computation in Chemistry, Berkeley, 1980) p. 13.
32. P. H. Berens and K. R. Wilson, J. Comp. Chem. 4, 313 (1983).
33. R. O. Watts and I. J. McGee, *Liquid State Chemical Physics* (Wiley-Interscience, New York, 1976).
34. R. A. Scott and H. A. Sheraga, J. Chem. Phys. 45, 2091 (1966).
35. G. Heublein, R. Kühmstedt, P. Kadura, and H. Dawczynski, Tetrahedron 26, 81 (1970).
36. K. P. Huber and G. Herzberg, *Constants of Diatomic Molecules* (Van Nostrand Reinhold, New York, N. Y., 1979).
37. J. C. Keck, Discuss. Faraday Soc. 33, 173 (1962).
38. J. C. Keck, Adv. Chem. Phys. 13, 85 (1967).
39. J. B. Anderson, J. Chem. Phys. 58, 4684 (1973).
40. J. B. Anderson, J. Chem. Phys. 62, 2446 (1975).
41. J. E. Straub, D. A. Hsu, and B. J. Berne, J. Chem. Phys. 89, 5188 (1985).
42. M. F. Herman and B. J. Berne, Chem. Phys. Lett. 77, 163 (1981).

43. K. E. Holdy, L. C. Klotz, and K. R. Wilson, J. Chem. Phys. **52**, 4588 (1970).
44. D. W. Oxtoby, in *Advances in Chemical Physics*, edited by S. A. Rice (John Wiley & Sons, New York, 1979) Vol. 40, p. 1.
45. D. W. Oxtoby, in *Advances in Chemical Physics*, edited by S. A. Rice (John Wiley & Sons, New York, 1981) Vol. 47, p. 487.
46. R. W. Zwanzig, Phys. Fl. **2**, 12 (1969).
47. R. F Grote and J. T. Hynes, J. Chem. Phys. **77**, 3736 (1982).
48. S. H. Northrup and J. T. Hynes, J. Chem. Phys. **73**, 2700 (1980).
49. J. P. Valleau and G. M. Torrie, J. Comput. Phys. **23**, 187 (1977).
50. G. M. White and K. R. Wilson, J. Chem. Phys. (submitted).
51. D. H. J. Mackay, P. M. Edelsten, and K. R. Wilson , (to be submitted).
52. J. C. Keck, Adv. At. Mol. Phys. **8**, 39 (1972).
53. D. Chandler, J. Chem. Phys. **68**, 2959 (1978).
54. J. A. Montgomery, D. Chandler, and B. J. Berne, J. Chem. Phys. **70**, 4056 (1979).
55. *ACS Symposium Series 263*, edited by D. G. Truhlar (American Chemical Society, Washington, D. C., 1984).
56. M. Simonyi and F. Tüdos, Adv. Phys. Org. Chem. **9**, 127 (1971).
57. E. S. Huyser, Adv. Free-Radical Chem. **1**, 77 (1965).
58. B. M. Ladanyi and J. T. Hynes, J. Am. Chem. Soc. **108**, 585 (1986).

Figure Captions

Figure 1. Potential energy LEPS surface contour plot as a function of the AB and BC bond lengths, r_1 and r_2, for a linear arrangement of X_3 with a barrier height of 20 kcal/mol, and with a barrier frequency of $\omega_b = 419$ cm^{-1}. The saddle point is indicated by a solid circle. The contour lines are labeled in units of kcal/mol. Note that the zero of the LEPS potential function is taken to be the potential energy of an isolated X_2 molecule at its equilibrium geometry.

Figure 2. Effective potential $\Phi'(\theta)$, $\Phi^{LEPS}(\theta)$ and the function $-k_BT\, ln[J(\theta)/r_1^2 r_2^2]$ as a function of θ for the 20 kcal/mol barrier of X_3 in which r_1 and r_2 are held constant at 2.254 Å.

Figure 3. Trajectory plots of X_3 on the 20 kcal/mol LEPS potential surface for the reaction in both liquid xenon (dashed line) and the gas phase (solid circles) with identical initial conditions chosen at time zero on the transition state surface, demonstrating the solvent effect on the details of the dynamics away from the transition barrier. The saddle point of the potential is indicated by a single solid circle.

Figure 4. Plot of the average energy versus time for the reaction $X + X_2 \rightarrow X_2 + X$ with the 20 kcal/mol energy barrier, for an ensemble of 126 reacting trajectories. Time zero is when the X_3 is first released at the saddle point. The solid lines show the average energy for the reaction in liquid argon solvent while the dots indicate the average energy for reaction in the absence of solvent (gas phase). The translational energy arises from and decays to the solvent in 0.2 ps, rotational in about 0.2 ps and, although the figure does not show this, vibrational energy in > 250 ps. Notice how translational and rotational energies are dumped into ABC potential energy to climb the steep barrier, and then dumped back into translation and rotation. The vibrational energy of the X_2 before and after barrier passage is approximately $3\,\hbar\omega$, where ω is the 560 cm^{-1} ground state vibrational angular frequency of X_2. Note that the average energies in the different modes for the gas and liquid phase reactions are approximately the same during the time period -0.05 ps to 0.05 ps during which the gas and liquid phase reaction trajectories are similar.

Figure 5. Solvent momentum sphere of influence on reaction with 20 kcal/mol barrier in argon solvent. For a chosen ensemble of 80 trajectories which react, the trajectories are carried back the period in time before the barrier crossing given on the horizontal axis. While holding all coordinates constant, all solvent atoms outside a sphere of radius measured from the center of mass of the X_3 atoms are randomized with a Boltzmann distribution in velocities. The trajectories are then allowed to resume. The probability on the vertical scale measures the fraction of trajectories which still lead to reaction. This gives a measure of the time and space scale over which solvent momenta play a role in the reaction.

Figure 6. Solvent friction on the reaction coordinate for the X_3 in a bent geometry (defined by the minimum in the effective potential, Φ', in Fig. 2) as function of time for the three inert solvents helium, argon and xenon, normalized by the value of the friction at time zero. The initial decay in the time dependent friction is approximated by a Gaussian Eq. (3.7) with values for τ of 0.06 ps, 0.19 ps, and 0.36 ps for He, Ar and Xe respectively, determined by numerically calculating the curvature of the time dependent friction at $t = 0$. The initial frictional frequencies, ω_ζ, for the three solvents are 15 cm^{-1}, 35 cm^{-1} and 40 cm^{-1} for He, Ar and Xe respectively.

Figure 7. Solvent friction on the linear geometry reaction coordinate as function of time for the three inert solvents helium, argon and xenon, normalized by the value of the friction at time zero. The initial frictional frequencies for the three solvents as well as the initial decay in the dependent friction are essentially the same as for the bent case in Fig. 6. The time dependent friction for the linear geometry, however, has a longer time decay than that for the bent geometry shown in Fig. 6.

Figure 8. The value of the transmission coefficient, κ, from Grote-Hynes theory as a function of barrier frequency, ω_b, in the solvents helium, argon, and xenon. The initial decay in the the time dependent frictions for these solvents (see Fig. 6) can be approximated by Gaussians Eq. (3.7), with values for τ of 0.06 ps, 0.19 ps, and 0.36 ps for He, Ar and Xe respectively. The Gaussian approximation is good for barrier frequencies greater than 50 cm^{-1} where the time spent on the barrier is short, but poor for barrier frequencies less than 50 cm^{-1} since the longer time friction becomes more important as the characteristic time spent on the barrier increases. For the reaction systems described in this work, the short time Gaussian approximation is adequate.

Figure 9. Illustration of the simple 3-stage picture to explain the essential features of the dynamics of A + BC reactions in rare gas solvents. The picture consists of three stages. Stage 1 is energy and phase arisal in reactants, stage 2 is approximately gas phase barrier crossing, while stage 3 is energy and phase decay of products in the solvent.

Figure 10. Schematic illustration of some predominant recrossing patterns observed in the MD simulation of A + BC reaction dynamics on low barriers in solution. The dividing line represents the transition barrier dividing surface between reactants on the left and products on the right, while the arrows indicate the direction of the trajectories for initially positive momentum: (a) is a direct, successful reactant $\rightarrow$ product transition with no recrossing; in TST, all initially forward trajectories are of this type; (b) is a single recrossing, reactant $\rightarrow$ product $\rightarrow$ reactant, after the transition barrier is crossed in the forward direction, and (c) is a single recrossing, product $\rightarrow$ reactant $\rightarrow$ product, in which the recrossing occurs prior to a reactant $\rightarrow$ product crossing.

Figure 11. Plot of the average energy versus time for the reaction $X + X_2 \rightarrow X_2 + X$ with the 5 kcal/mol energy barrier, for an ensemble of 64 trajectories. Time zero is when the X_3 is first released at the saddle point. The solid lines show the average energy for the reaction in liquid argon solvent while the dots indicate the average energy for a reaction in the absence of solvent (gas phase). The translational and rotational energies arise from and decay to the solvent in approximately 0.5 ps, and, although the figure does not show this, the vibrational energy arises and decays in > 250 ps.

Figure 12. Plot of the average energy versus time for the reaction $X + X_2 \rightarrow X_2 + X$ with the 20 kcal/mol energy barrier, for an ensemble of 64 reacting trajectories. Time zero is when the X_3 is first released at the saddle point. The solid lines show the average energy for the reaction in liquid helium solvent while the dots indicate the average energy for a reaction in the absence of solvent (gas phase). The translational and rotational energy arises from and decays to the solvent over a time scale measuring longer than 1.0 ps, and, although the scale of the figure does not show it, vibrational energy starts to decay appreciably in less than 10 ps.

Figure 13. Plot of the average energy versus time for the reaction $X + X_2 \rightarrow X_2 + X$ with the 20 kcal/mol energy barrier, for an ensemble of 252 trajectories. Time zero is when the X_3 is first released at the saddle point. The solid lines show the average energy for the reaction in liquid xenon solvent while the dots indicate the average energy for a reaction in the absence of solvent (gas phase). The

translational energy arises from and decays to the solvent in 0.15 ps, and, although the figure does not show this, vibrational energy starts to decay in > 100 ps.

Figure 14. Plot of the average energy versus time for the reaction $X + X_2 \rightarrow X_2 + X$ with the 5 kcal/mol energy barrier, for an ensemble of 64 trajectories. Time zero is when the X_3 is first released at the saddle point. The solid lines show the average energy for the reaction in liquid helium solvent while the dots indicate the average energy for a reaction in the absence of solvent (gas phase). The translational and rotational energy arises from and decays to the solvent over a time scale measuring longer than 1.0 ps, and, although the figure does not show this, vibrational starts to transform in less than 10 ps.

Figure 15. Plot of the average energy of versus time for the reaction $X + X_2 \rightarrow X_2 + X$ with the 5 kcal/mol energy barrier, for an ensemble of 252 trajectories. Time zero is when the X_3 is first released at the saddle point. The solid lines show the average energy for the reaction in liquid xenon solvent while the dots indicate the average energy for a reaction in the absence of solvent (gas phase). The translational energy arises from and decays to the solvent in 0.15 ps, and, although the figure does not show this, vibrational energy starts to transform in > 100 ps.

Figure 16. Solvent momentum sphere of influence on reaction with the 20 kcal/mol barrier in helium solvent. For details, see the caption of Fig. 5.

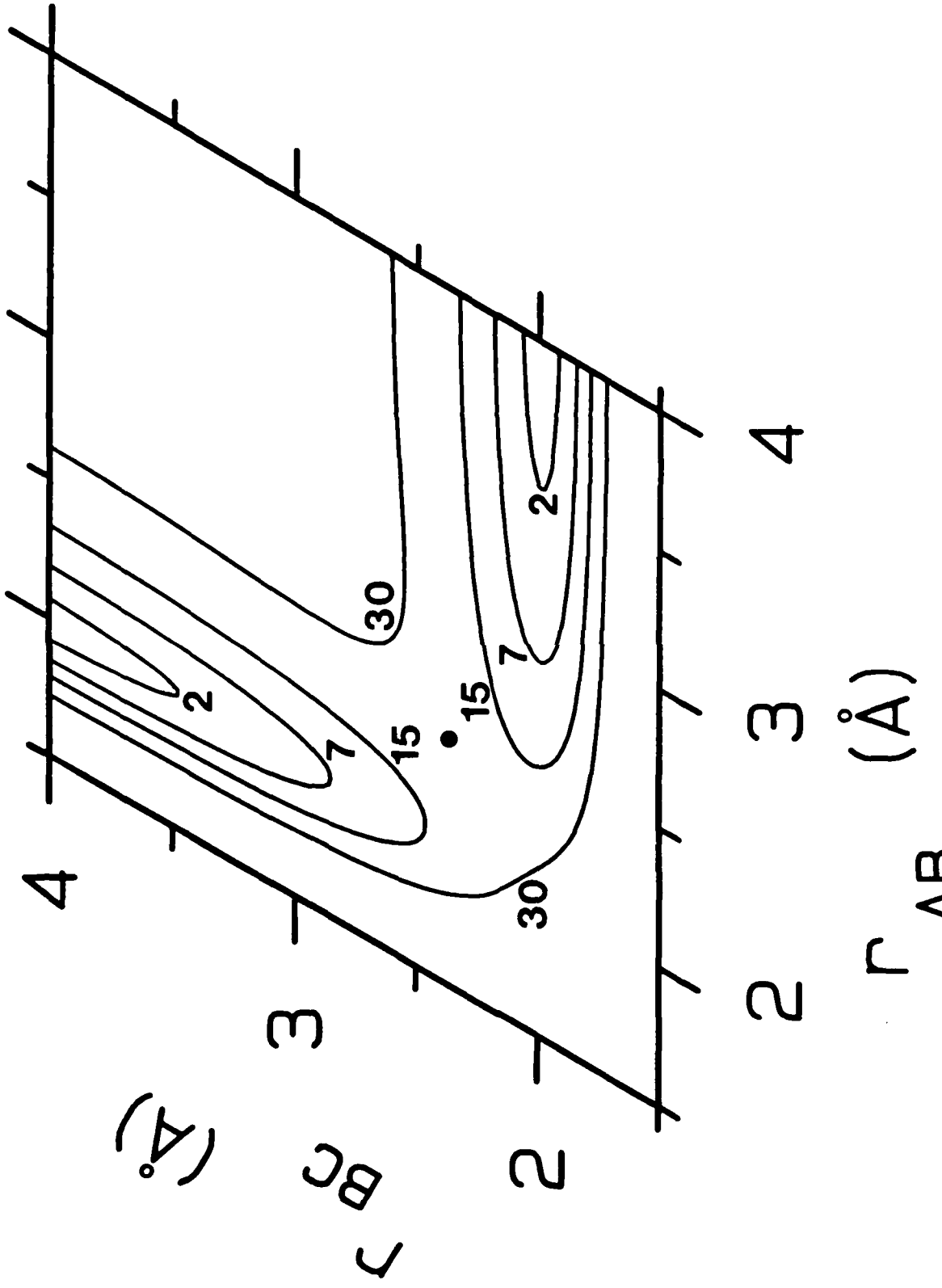

FIGURE 1

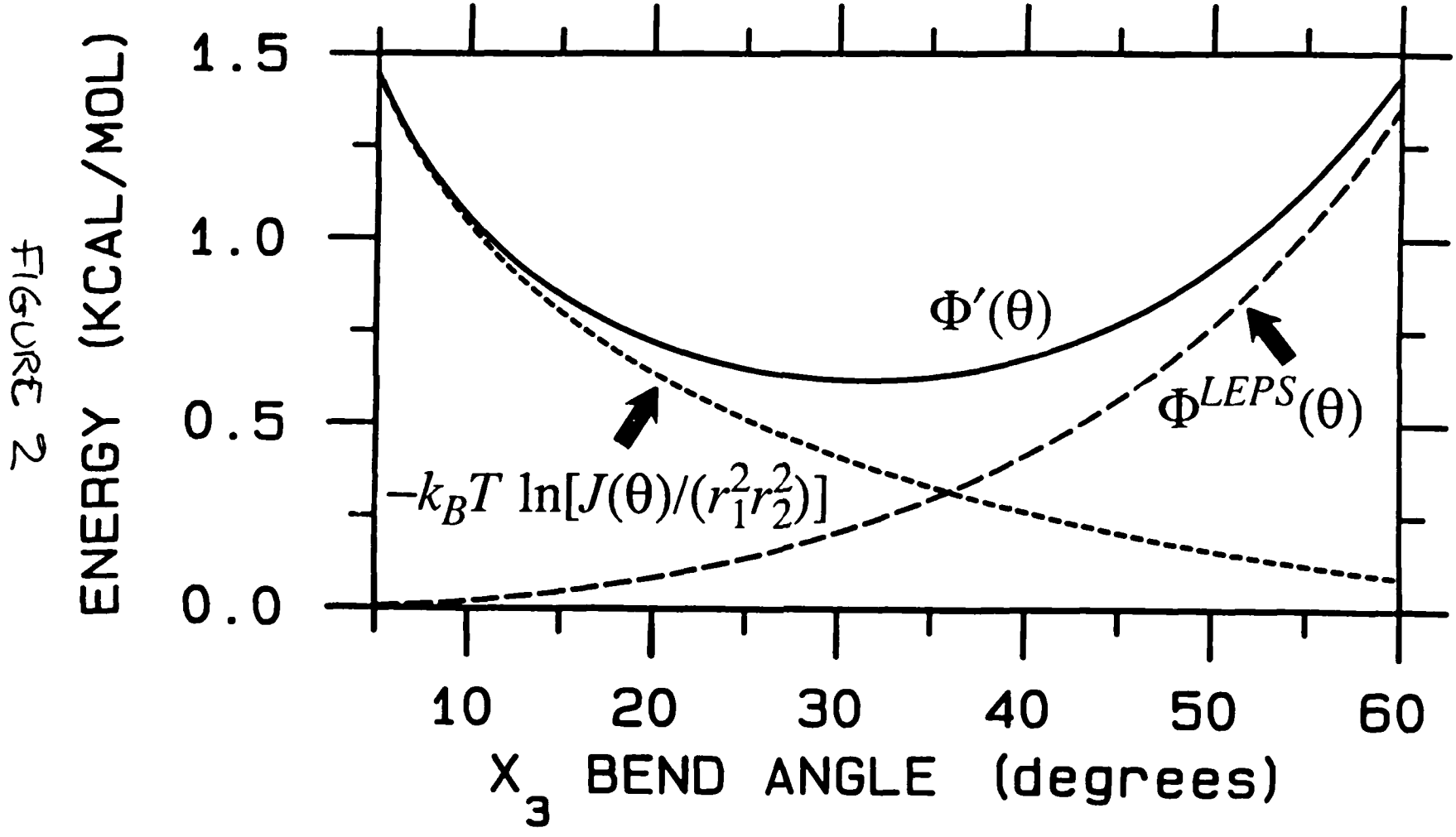
BEND POTENTIAL FOR X3
ENERGY (KCAL/MOL)
1.5
1.0
0.5
0.0
10
20
30
40
50
60
X3 BEND ANGLE (degrees)
Φ′(θ)
Φ^LEPS(θ)
−k_B T ln[J(θ)/(r1^2 r2^2)]

FIGURE 2

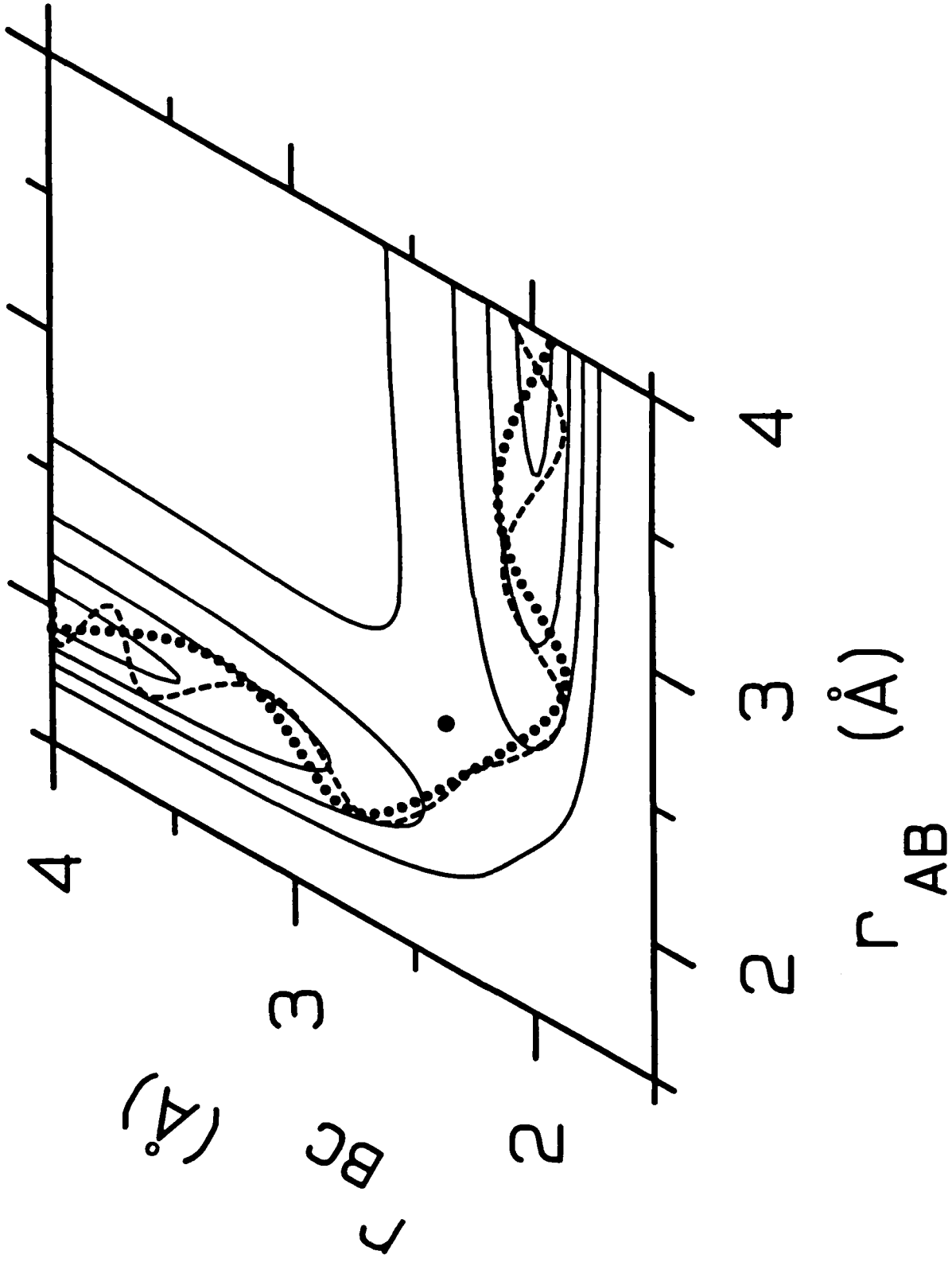

FIGURE 3

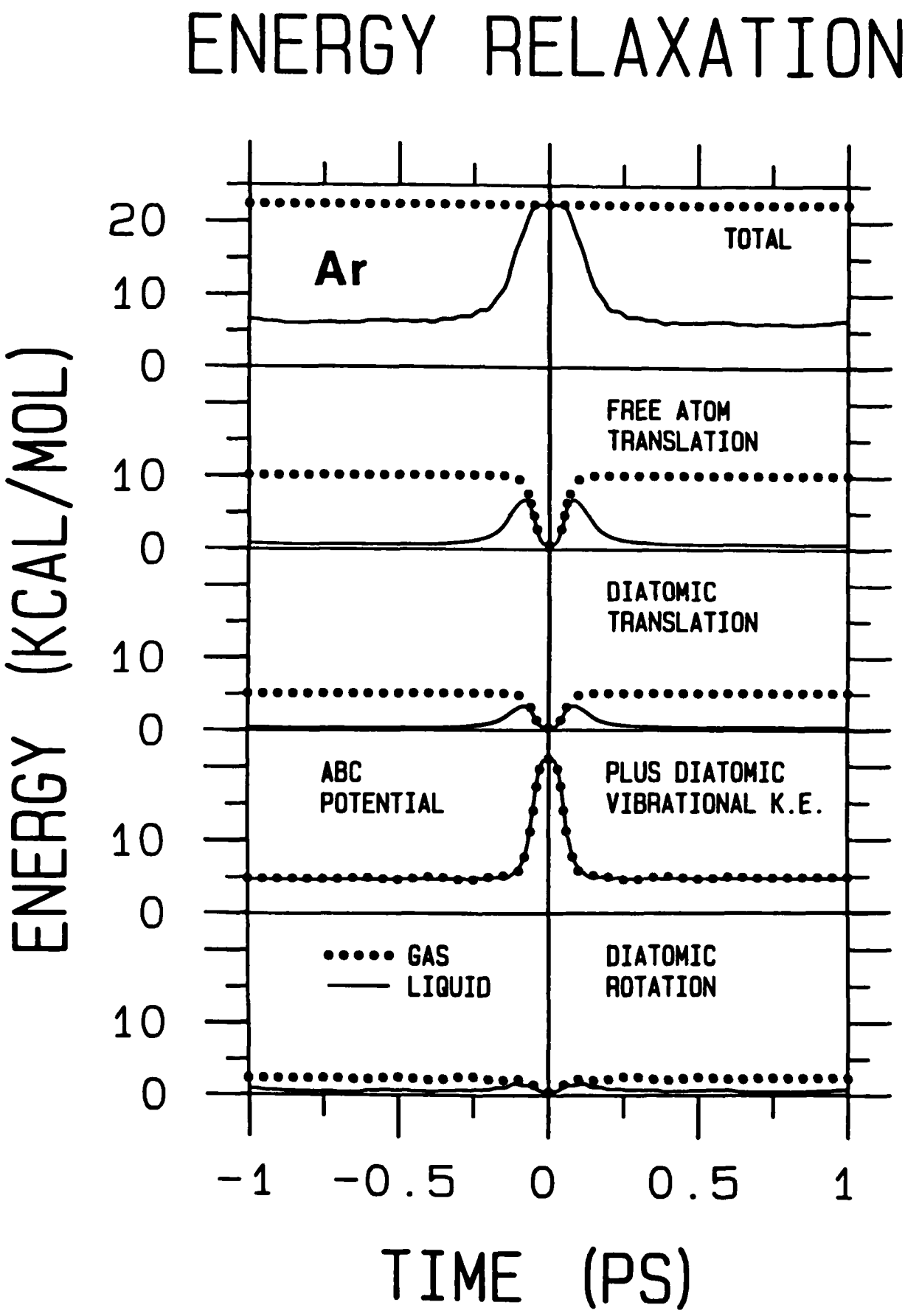
ENERGY RELAXATION
Ar
TOTAL
FREE ATOM
TRANSLATION
DIATOMIC
TRANSLATION
ABC
POTENTIAL
PLUS DIATOMIC
VIBRATIONAL K.E.
GAS
LIQUID
DIATOMIC
ROTATION
ENERGY (KCAL/MOL)
20
10
0
10
0
10
0
10
0
10
0
-1
-0.5
0
0.5
1
TIME (PS)

FIGURE 4

20 kcal/mol, Ar
PROBABILITY
0
0.5
1
0.0
0.1
0.2
0.3
TIME (ps)
0
2
4
6
RADIUS (Å)

FIGURE 5

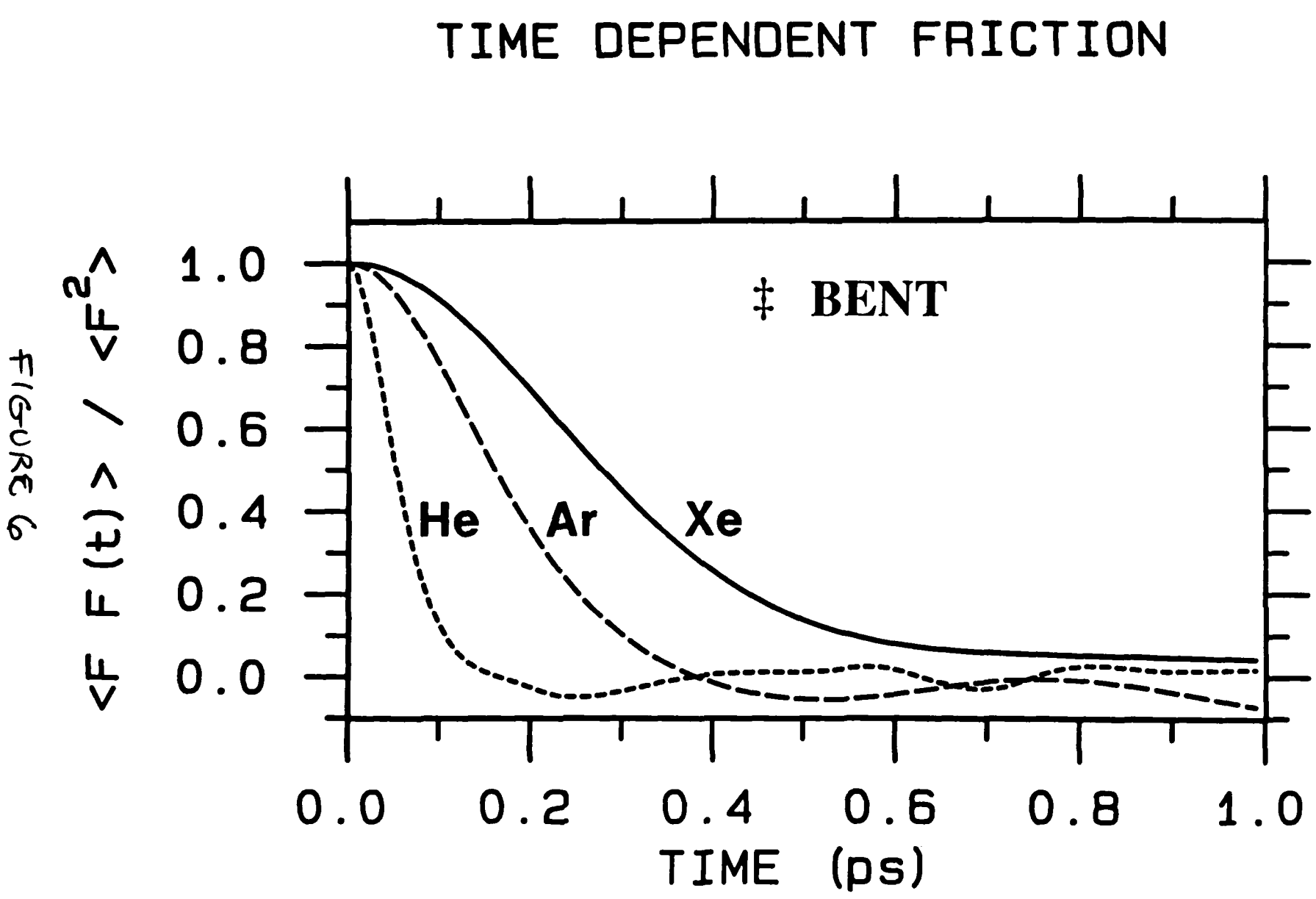
TIME DEPENDENT FRICTION
‡ BENT
He
Ar
Xe
<F F(t) > / <F2>
1.0
0.8
0.6
0.4
0.2
0.0
0.0
0.2
0.4
0.6
0.8
1.0
TIME (ps)

FIGURE 6

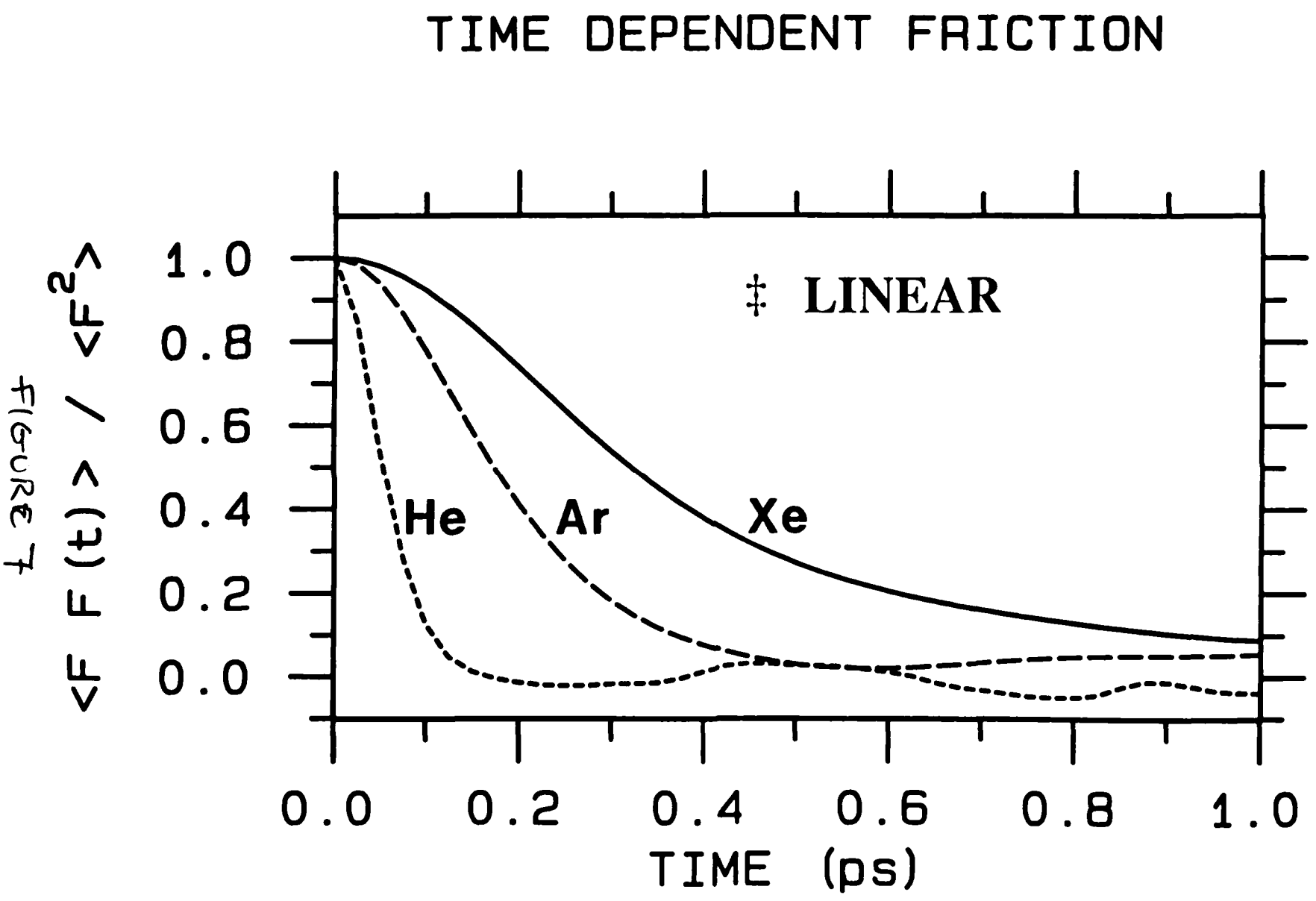
TIME DEPENDENT FRICTION
‡ LINEAR
He
Ar
Xe
<F F(t)> / <F²>
1.0
0.8
0.6
0.4
0.2
0.0
0.0
0.2
0.4
0.6
0.8
1.0
TIME (ps)

FIGURE 7

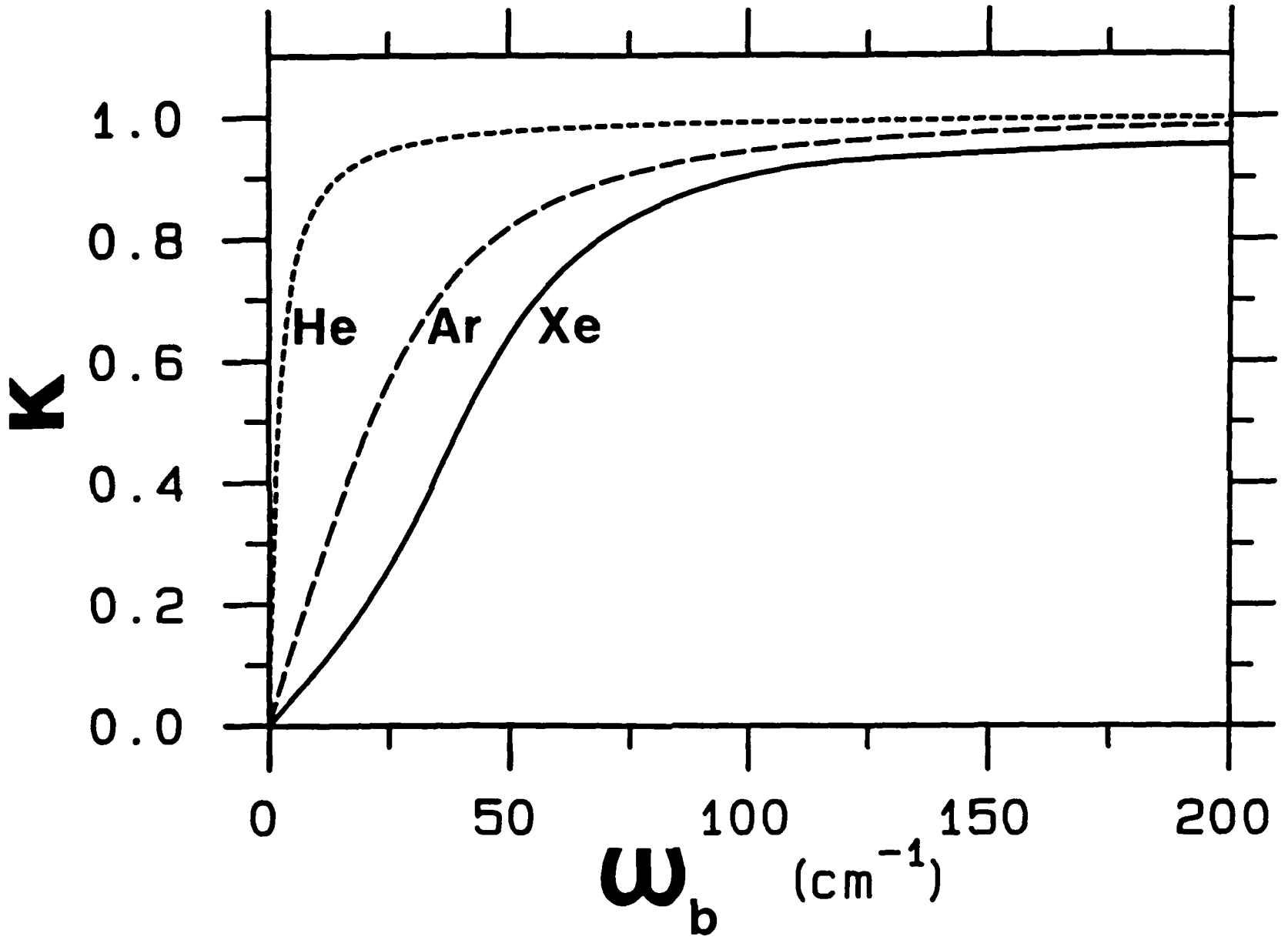

FIGURE 8

SIMPLE 3-STAGE PICTURE

STAGE 1

ENERGY AND
PHASE ARISAL

STAGE 2

BARRIER CROSSING:
APPROXIMATELY GAS
PHASE DYNAMICS

STAGE 3

ENERGY AND
PHASE DECAY

FIGURE 9

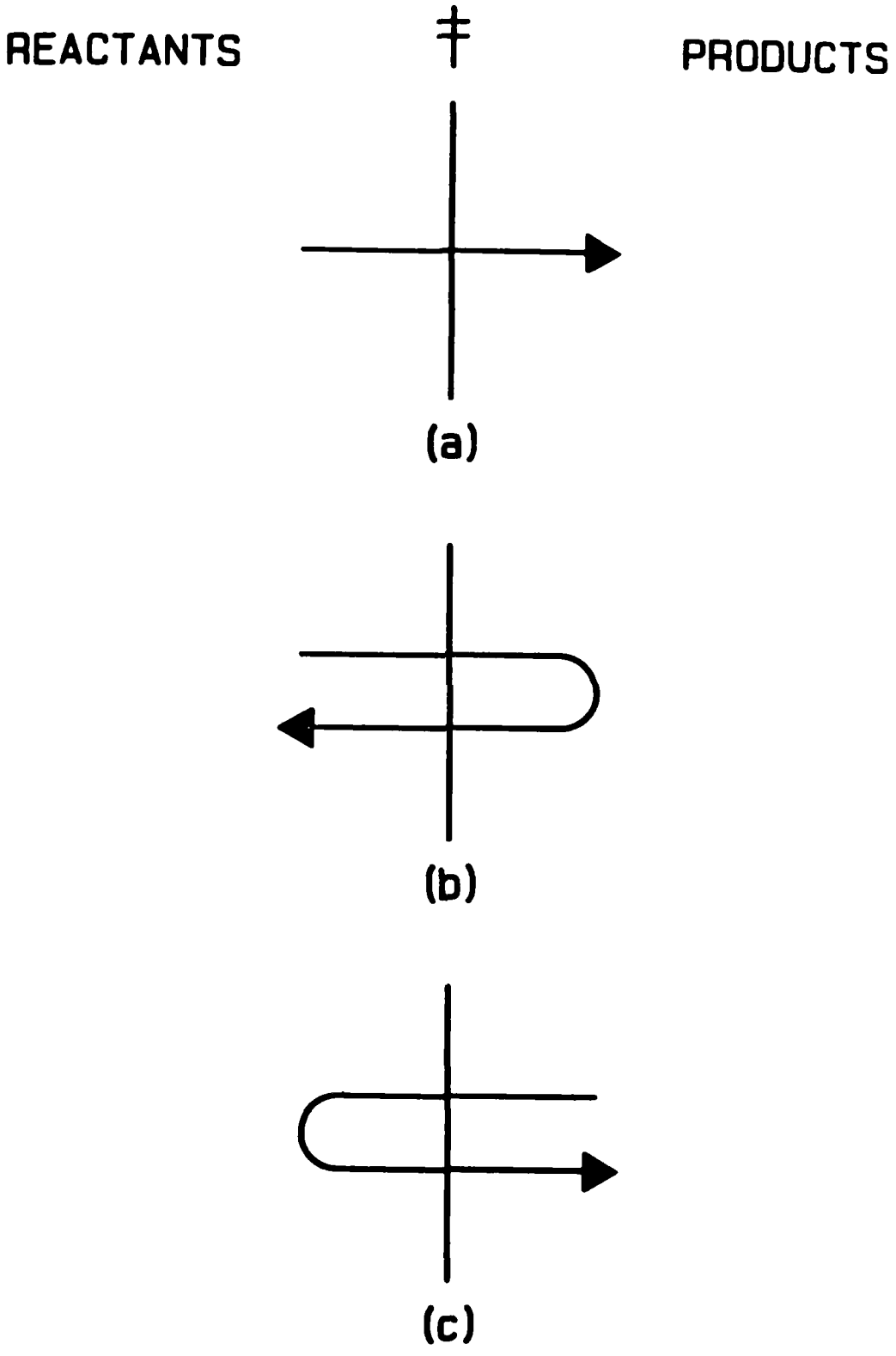

FIGURE 10

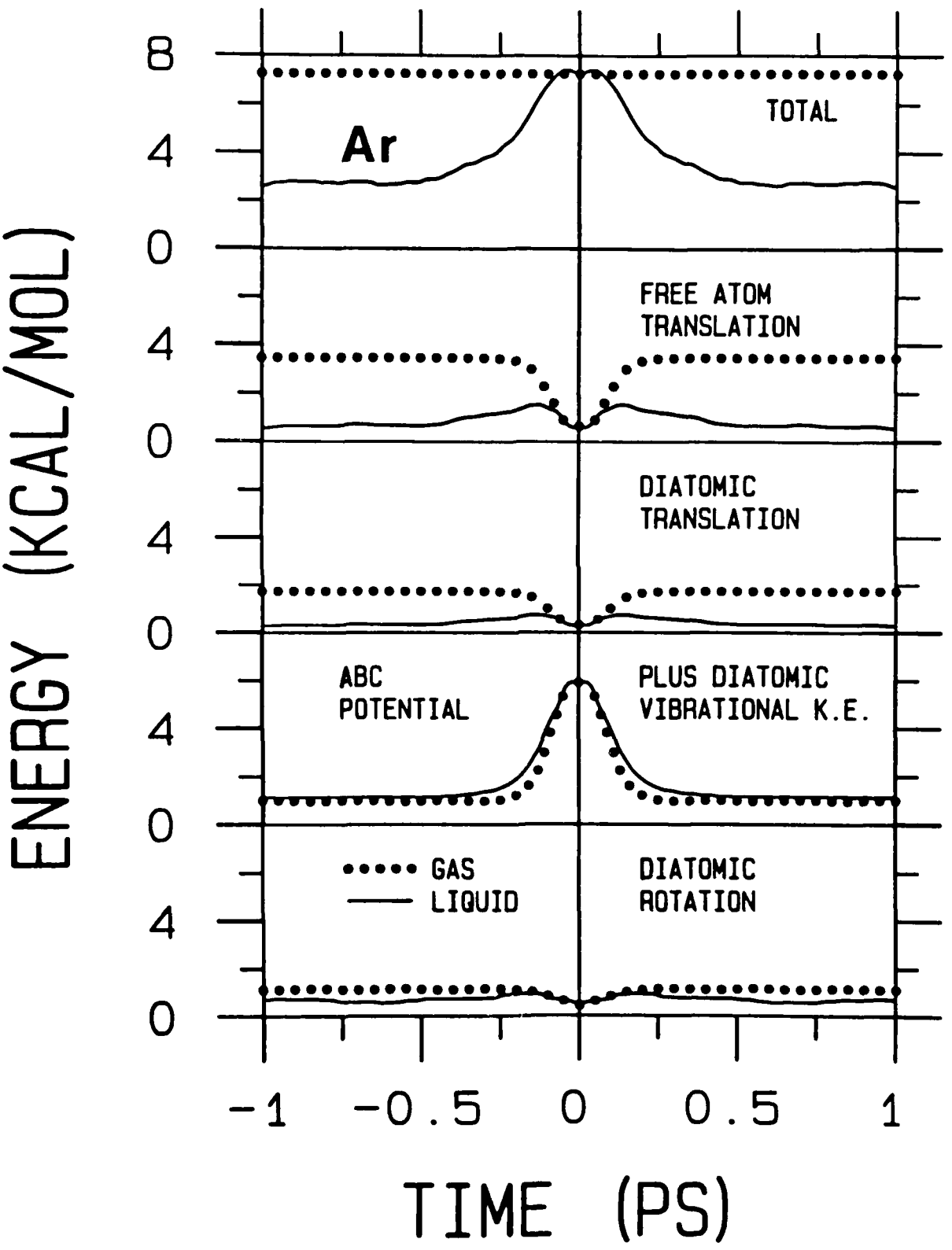
ENERGY RELAXATION
ENERGY (KCAL/MOL)
8
4
0
4
0
4
0
4
0
Ar
TOTAL
FREE ATOM
TRANSLATION
DIATOMIC
TRANSLATION
ABC
POTENTIAL
PLUS DIATOMIC
VIBRATIONAL K.E.
GAS
LIQUID
DIATOMIC
ROTATION
-1
-0.5
0
0.5
1
TIME (PS)

FIGURE 11

ENERGY RELAXATION

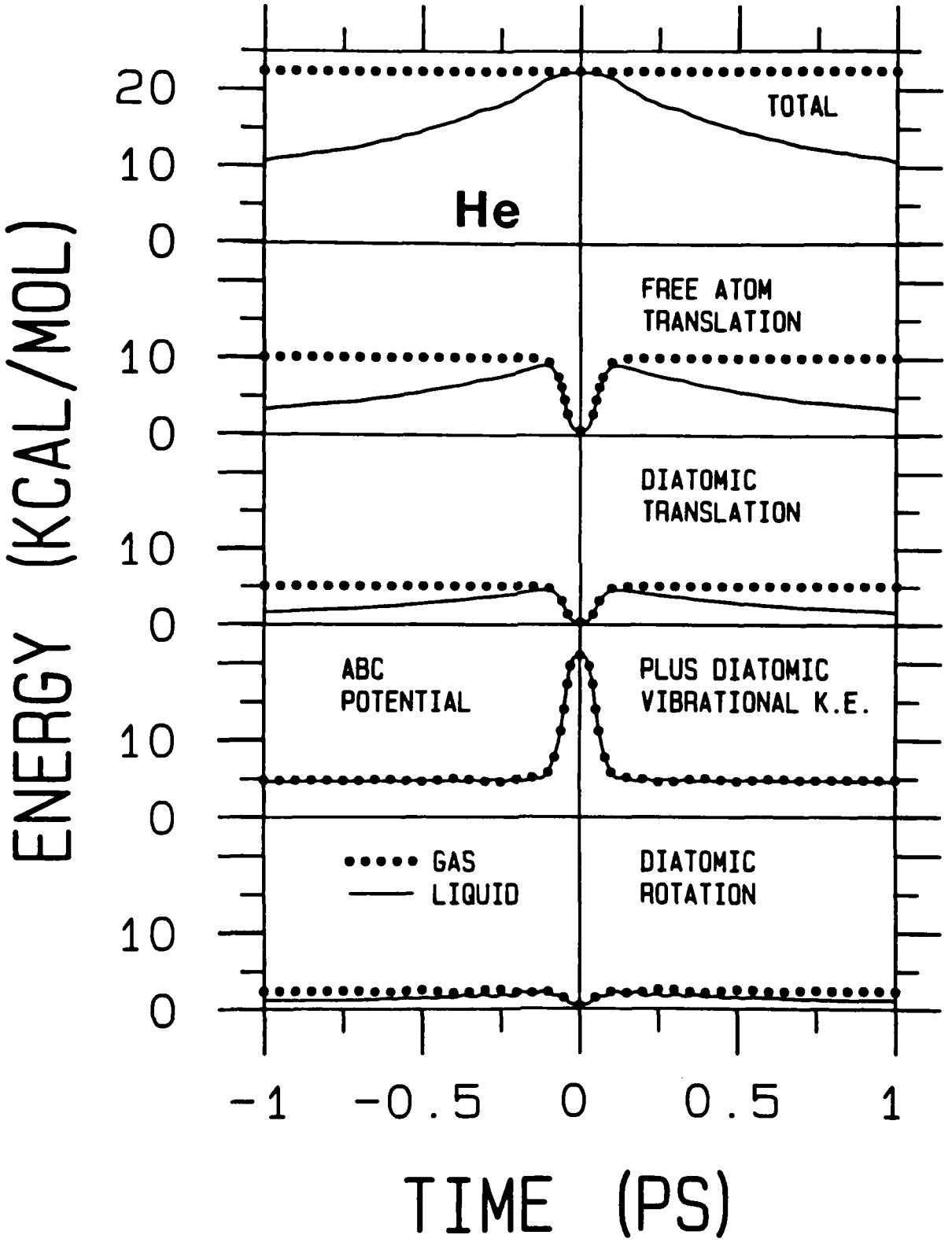

FIGURE 12

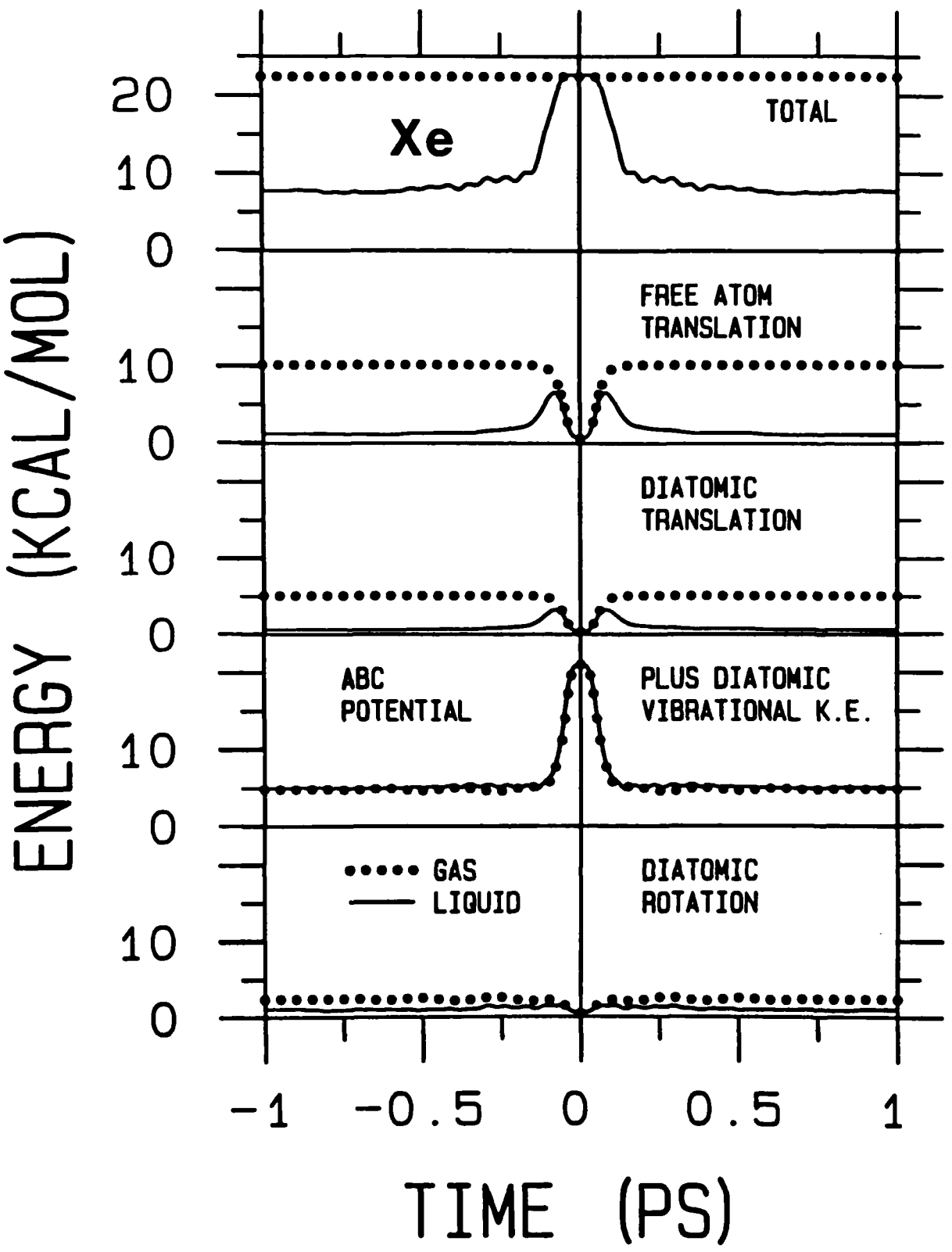
ENERGY RELAXATION
Xe
TOTAL
FREE ATOM
TRANSLATION
DIATOMIC
TRANSLATION
ABC
POTENTIAL
PLUS DIATOMIC
VIBRATIONAL K.E.
GAS
LIQUID
DIATOMIC
ROTATION
ENERGY (KCAL/MOL)
20
10
0
10
0
10
0
10
0
10
0
-1
-0.5
0
0.5
1
TIME (PS)

FIGURE 13

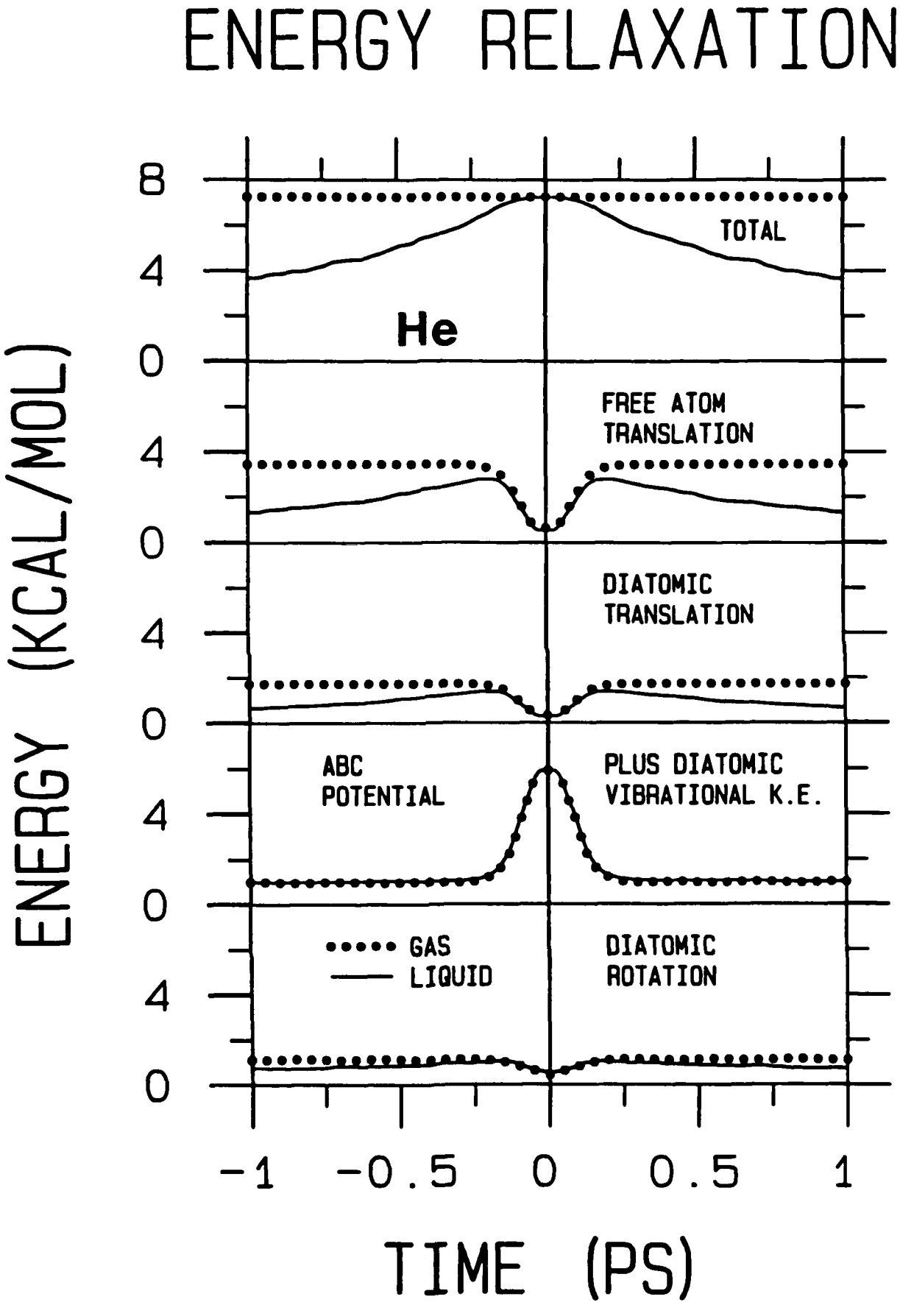
ENERGY RELAXATION
ENERGY (KCAL/MOL)
8
4
0
4
0
4
0
4
0
TOTAL
He
FREE ATOM
TRANSLATION
DIATOMIC
TRANSLATION
ABC
POTENTIAL
PLUS DIATOMIC
VIBRATIONAL K.E.
GAS
LIQUID
DIATOMIC
ROTATION
-1
-0.5
0
0.5
1
TIME (PS)

FIGURE 14

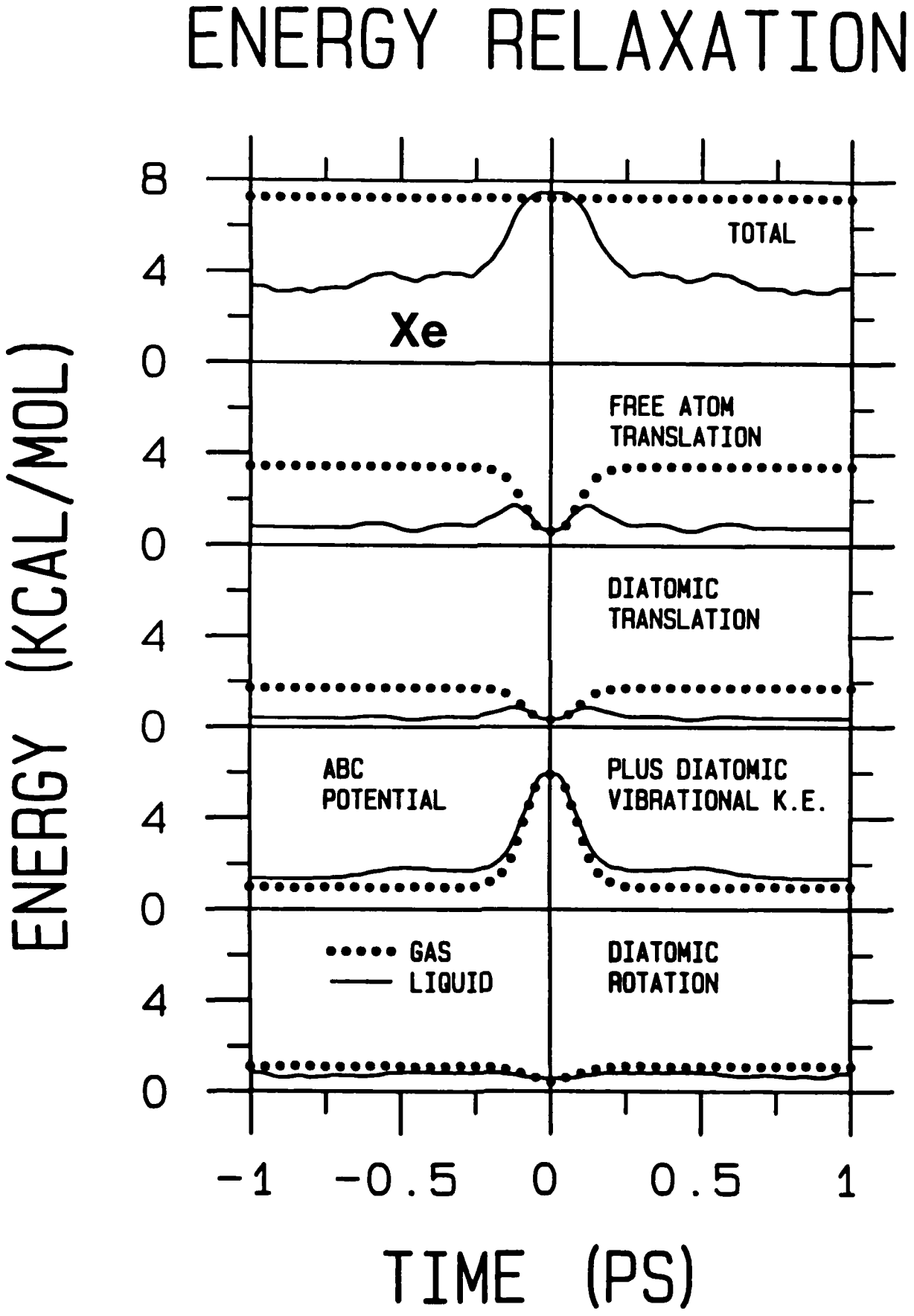
ENERGY RELAXATION
ENERGY (KCAL/MOL)
8
4
0
4
0
4
0
4
0
TOTAL
Xe
FREE ATOM
TRANSLATION
DIATOMIC
TRANSLATION
ABC
POTENTIAL
PLUS DIATOMIC
VIBRATIONAL K.E.
GAS
LIQUID
DIATOMIC
ROTATION
-1
-0.5
0
0.5
1
TIME (PS)

FIGURE 15

20 kcal/mol, He
PROBABILITY
0 0.5 1
0.0 0.1 0.2 0.3
TIME (ps)
0 2 4 6 8
RADIUS (Å)

FIGURE 16

END

DTIC

6-86